Advances in Water Resources 33 (2010) 969–986

Contents lists available at ScienceDirect

Advances in Water Resources

journal homepage: www.elsevier.com/ locate/advwatres

Biological reduction of chlorinated solvents: Batch-scale geochemical modeling

Irina Kouznetsova [a], Xiaomin Mao [b], Clare Robinson [c,1], D.A. Barry [c], Jason I. Gerhard [a,*,1], Perry L. McCarty [d]

[a] Institute for Infrastructure and Environment, University of Edinburgh, Edinburgh, EH9 3JL, UK
[b] College of Water Conservancy and Civil Engineering, China Agricultural University, Beijing, 100083, China
[c] Laboratoire de technologie écologique, Institut d'ingénierie de l'environnement, Faculté de l'environnement naturel, architectural et construit, Station No. 2, Ecole Polytechnique Fédérale de Lausanne (EPFL), CH-1015 Lausanne, Switzerland
[d] Department of Civil and Environmental Engineering, Environment and Engineering Building, 473 Via Ortega, MC 4020, Room 259, Stanford University, Stanford, CA 94305, USA

ARTICLE INFO

Article history:
Received 29 August 2009
Received in revised form 29 April 2010
Accepted 30 April 2010
Available online 7 May 2010

Keywords:
Modeling
Groundwater
Bioremediation
Chlorinated ethenes
Biogeochemical reactions
Sensitivity analysis

ABSTRACT

Simulation of biodegradation of chlorinated solvents in dense non-aqueous phase liquid (DNAPL) source zones requires a model that accounts for the complexity of processes involved and that is consistent with available laboratory studies. This paper describes such a comprehensive modeling framework that includes microbially mediated degradation processes, microbial population growth and decay, geochemical reactions, as well as interphase mass transfer processes such as DNAPL dissolution, gas formation and mineral precipitation/dissolution. All these processes can be in equilibrium or kinetically controlled. A batch modeling example was presented where the degradation of trichloroethene (TCE) and its byproducts and concomitant reactions (e.g., electron donor fermentation, sulfate reduction, pH buffering by calcite dissolution) were simulated. Local and global sensitivity analysis techniques were applied to delineate the dominant model parameters and processes. Sensitivity analysis indicated that accurate values for parameters related to dichloroethene (DCE) and vinyl chloride (VC) degradation (i.e., DCE and VC maximum utilization rates, yield due to DCE utilization, decay rate for DCE/VC dechlorinators) are important for prediction of the overall dechlorination time. These parameters influence the maximum growth rate of the DCE and VC dechlorinating microorganisms and, thus, the time required for a small initial population to reach a sufficient concentration to significantly affect the overall rate of dechlorination. Self-inhibition of chlorinated ethenes at high concentrations and natural buffering provided by the sediment were also shown to significantly influence the dechlorination time. Furthermore, the analysis indicated that the rates of the competing, nonchlorinated electron-accepting processes relative to the dechlorination kinetics also affect the overall dechlorination time. Results demonstrated that the model developed is a flexible research tool that is able to provide valuable insight into the fundamental processes and their complex interactions during bioremediation of chlorinated ethenes in DNAPL source zones.

1. Introduction

Chlorinated ethenes are among the most common organic groundwater contaminants because of their wide use, and uncontrolled disposal and improper management [105]. Often released in substantial quantities, they are frequently present in the subsurface as dense non-aqueous phase liquids (DNAPLs). In a solvent DNAPL source zone, aqueous phase chlorinated ethenes continuously dissolve into groundwater, resulting in an aqueous phase plume emanating downgradient. Such plumes are of concern due to the carcinogenic and mutagenic potential of chlorinated solvents [97,113].

In situ biodegradation is an attractive technique for the treatment of chlorinated ethenes in soil and groundwater [83]. Under anaerobic conditions, tetrachloroethene (PCE) and trichloroethene (TCE) can be degraded by metabolic reductive dechlorination (i.e., dechlororespiration) in a sequential manner to less chlorinated compounds: dichloroethene (DCE), vinyl chloride (VC), and non-toxic ethene (ETH) [59]. The dechlorination process relies on the presence of electrons, whereby the chlorinated compound is used by microbes as the terminal electron acceptor and hydrogen (H_2) as the electron donor (e-donor). Other compounds can potentially serve as direct e-donor (e.g., acetate and formate), however their utilization depends on the microbial species involved and therefore may not occur readily [8,37,92]. Although direct addition of H_2 is possible in the field [1], H_2 is typically added indirectly by the injection of fermentable (primary) organic substrates (e.g., lactate, ethanol, pentanol, glucose, soybean oil) [35,59]. In the absence of external e-donors, biomass decay can slowly release H_2 sufficient to

* Corresponding author.
E-mail addresses: irina.kouznetsova@ed.ac.uk (I. Kouznetsova), maoxiaomin@tsinghua.org.cn (X. Mao), crobinson@eng.uwo.ca (C. Robinson), andrew.barry@epfl.ch (D.A. Barry), jgerhard@eng.uwo.ca (J.I. Gerhard), pmccarty@stanford.edu (P.L. McCarty).
[1] Present address: Department of Civil and Environmental Engineering, University of Western Ontario, London, Canada N6A 5B9.

0309-1708/$ – see front matter © 2010 Elsevier Ltd. All rights reserved.
doi:10.1016/j.advwatres.2010.04.017

support dechlorination [96,110], referred to as endogenous respiration [66].

Rapid and complete dechlorination may be impeded by alternative terminal electron-accepting processes (TEAPs) competing with reductive dechlorinators for H_2 and short-chain fatty acids [16]. Competing microbial populations include denitrifiers, methanogens, acetogens, sulfate reducers and iron-reducers. Iron and sulfate are the most important alternative electron acceptors due to their ubiquity in aquifer systems and the similarity of the H_2 threshold for their respective TEAPs: ~2 nM for dechlorination [108], 0.1–0.8 nM for iron reduction [55], 1–4 nM for sulfate reduction [17,56].

Reductive dechlorination within DNAPL source zones is of particular interest as recent studies have demonstrated the ability of microbial isolates [4] and mixed dechlorinating consortia [15,34,67,109] to dechlorinate PCE at (or near) saturated aqueous phase concentrations to ETH. Additional benefits of source zone bioremediation include (i) reduced DNAPL longevity due to enhanced DNAPL dissolution [4,18,90,109,111], and (ii) toxic inhibition of microbial communities competing for e-donor (e.g., homoacetogens and methanogens [36,108]). In addition, employing substrates that partition into the DNAPL phase (e.g., emulsified vegetable oil) provides a long-term source of e-donor for biodegradation [111]. 'Enhanced' bioremediation refers to the addition of nutrients and/or dechlorinating microbial cultures to the subsurface to initiate or accelerate the process [59].

Descriptions of biodegradation of chlorinated ethenes in DNAPL source zones have focused on the main reactants, i.e., chlorinated ethenes, (fermentable) e-donor, and competing TEAPs (e.g., [4,19,36,48]). However, geochemical interactions occur also—both in response to biodegradation reactions and independently—and may play a critical role in the dechlorination process (e.g., [9]). Each dechlorination step produces one chloride ion, giving rise to hydrochloric acid (HCl) production. The combination of this strong acid and build-up of short-chain fatty acids formed during e-donor fermentation can result in significant groundwater acidification [2,21,72]. The pH may be partially buffered through the dissolution of calcite and iron oxides (e.g., goethite FeOOH, ferrihydrite $Fe(OH)_3$). However, the natural soil buffering capacity may be limited, and acidic conditions can inhibit microbial activity. Laboratory studies have demonstrated that the optimal pH range for anaerobic microbes is from 6.5 to 7.5 [54] and low pH has been shown to reduce microbial reaction rates [2,27,51,117]. The influence of pH on biodegradation is expected to be of particular importance during the treatment of DNAPL source zones, as opposed to chlorinated ethene plumes, due to the higher total mass of dechlorination and fermentation products generated.

Numerical models of varying sophistication have been developed to simulate the biodegradation of chlorinated ethenes and associated reactions. Table 1 summarizes the characteristics and capabilities of existing models, as well as the model presented here. A number of models assume direct addition of H_2 [4,22,31], while others include the fermentation of typical organic substrates used in field applications [6,19,35,48]. Competition for e-donor with TEAPs is neglected in models simulating systems with high levels of uniform contamination or laboratory studies with pure cultures [4,31]. However, systems with complex microbial ecology and non-uniform contaminant distribution require the simulation of competition for e-donor [6,19,36,48,107]. Some models have included competition between chlorinated ethenes [4,22,31,32], often assuming that the presence of more chlorinated ethenes exclusively inhibits the dechlorination of less chlorinated ethenes [107,115,116]. Self-inhibition (also known as Haldane inhibition) associated with high chlorinated ethene concentrations (up to 1000 μM) has also been considered in some models [4,58,115]. Dechlorination kinetics have been approximated by first order [15,25], Michaelis-Menten [41] and Monod-type rate equations [19,21,31,32]. In Michaelis-Menten and Monod-type formulations the dechlorination rate is limited by e-donor availability [4,6,22,36]. Several models include interphase mass transfer processes such as DNAPL dissolution [4,15,19,20,74,107] or transfer of H_2 from the gas to aqueous phase [22] while two have considered endogenous respiration [36,48]. None of the available dechlorination models have incorporated geochemical processes (e.g., mineral interactions, pH, and alkalinity).

This paper presents a general framework for modeling enhanced DNAPL source zone bioremediation that includes the interaction of key physical, biological and geochemical processes. The main goal is to use the model to assess dechlorination complexity and process feedbacks. As outlined in Table 1, the model accounts for e-donor fermentation, dechlorination of chlorinated ethenes, competing TEAPs (e.g., sulfate and iron reduction), growth and decay of multiple microbial communities, pH and alkalinity, mineral precipitation/dissolution, gas formation, and mass transfer of species between non-aqueous and aqueous phases. Although other complex models with comparable features exist, for example models that integrate the dependency of the reaction kinetics on the concentration of solutes [24,91], explicitly simulate growth and decay of bacteria [79] and account for pH-dependent bacterial growth [11], these complex biogeochemical models were applied in systems such as landfill leachate aquifer plumes and BTEX (benzene, toluene, ethylbenzene and xylene) spills [11,12,77–79,86]. The presented model is the first that accounts explicitly for reductive dechlorination by microbial communities as well as detailed soil–water geochemistry. In addition, it differs to most of the previous biogeochemical models, in which the organic substrate (contaminant) is consumed via a sequence of electron acceptors (redox zonation), since here the fermentation of organic substrate (e-donor) occurs simultaneously with the consumption of competing electron acceptors including the reduced chlorinated ethenes. This work provides an example of the interaction of the biological and geochemical processes in a base case simulation of a hypothetical batch system with high, aqueous phase chlorinated solvent concentrations. Subsequently, sensitivity analyses are performed to determine the dominant model parameters and processes in the system and their influence on the various subsets of reaction complexities.

2. Numerical model

Fig. 1 presents the main processes involved in the anaerobic degradation of chlorinated ethenes. For each process from Fig. 1 included in the model the associated reactions are provided in Table 2 (see corresponding process number). As illustrated in Fig. 1, microbially mediated fermentation and degradation processes are linked in the model by dynamic hydrogen concentrations. In addition, the model accounts for all relevant acid and alkalinity-associated reactions (e.g., aqueous speciation, gas formation, mineral interactions) to track pH and the subsequent effects on microbial populations. In this section, the various processes given in Fig. 1 are described mathematically.

The fermentation of an organic substrate (process 1 in Fig. 1) is generally described by Eq. (1) (Table 2). The stoichiometric yield coefficients for H_2, acetate (CH_3COOH) and CO_2 (x, y, and z, respectively) for commonly used substrates are provided in Table 3. The concentrations of H_2 generated can differ by orders of magnitude depending on H_2-production ceilings of the specific fermentation reaction (i.e., maximum levels of H_2 that can be achieved via fermentation [36]). This is accounted for in the model by an H_2 inhibition term. The intermediate products identified by Eq. (1) refer to the breakdown of complex substrates into compounds with simpler structures (e.g., volatile fatty acids, Table 3).

In the model, fermentation kinetics is expressed as:

$$\frac{dC_{ps}}{dt} = -k_{max}^{ps} X_{FB} \left(\frac{C_{ps}}{K_S^{ps} I_{CI} + C_{ps}} \right) F(pH) \phi(H_2) \left(1 - \frac{C_{H_2S}}{K_1^{H_2S}} \right), \quad (17)$$

Table 1
Overview of the existing models simulating reductive dechlorination in groundwater.

References	Processes considered													
	Fermentable substrates	Direct e-donor(s)	E-donor limitation	Chlorinated ethene(s)	Dechlorination kinetics	Nonchlorinated TEAPs	Competitive, product- and self-inhibition	pH inhibition of microbial activity	H_2 from biomass decay	Bioclogging	Gas formation	NAPL dissolution	Mineral dissolution and precipitation	Transport
Present study	Linoleic acid	H_2 (from fermentation and acetate oxidation)	√	TCE–DCE–VC	Monod kinetics (with biomass growth and decay)	Sulfate reduction	DCE by TCE, VC by DCE, Linoleic acid by TCE, self-inhibition of chlorinated ethenes, inhibition of all microbes by H_2S	√	–	–	√	√	√	–
Sleep and Sykes [94,95]	–	–	–	PCE–TCE–DCE-VC	First-order kinetics	–	–	–	–	–	√	√	–	√
Tandoi et al. [100]	–	Methanol	–	PCE–TCE–DCE-VC	Zero- and first-order kinetics	–	VC inhibited by the other chlorinated ethenes (except trans-DCE)		–	–	–	–		–
Bagley [6]	Ethanol	H_2	√	PCE–TCE–DCE-VC	Monod kinetics (with biomass growth and decay)	Acetogenesis and methanogenesis	Inhibition of VC by other chlorinated ethenes, inhibition of H_2 consumption by PCE	–	–	–	–	–	–	–
Fennell and Gossett [36]	Butyric acid, ethanol, lactic acid, propionic acid	H_2	√	PCE	Monod kinetics (with biomass growth and decay)	Methanogenesis	–	–	√	–	√		–	–
Haston and McCarty [41]	–	–	–	PCE–TCE–DCE–VC	Michaelis-Menten kinetics	–	–	–	–	–	–	–	–	–
Carr et al. [15]	–	–	–	PCE–TCE–DCE	First-order kinetics	–	–	–	–	–	–	√	–	–
Clement et al. [25]	–	–	–	PCE–TCE–DCE-VC	First-order kinetics	–	–		–	–	–	–		√
Chu et al. [20]	–	Acetate	√	PCE–DCE	Monod kinetics (with biomass growth and decay)	–	–		–	√	–	√		√
Chu et al. [21]	–	?	√	PCE–TCE–DCE	Monod kinetics (with biomass growth and decay)	√	Between PCE and TCE	–	–	√	–	√		√
Clapp et al. [22]	–	H_2	√	PCE–TCE–DCE-VC	Monod kinetics (with biomass growth and decay)	Methanogenesis	PCE by TCE, TCE by PCE, DCE by VC, VC by DCE	–	–	–	√	–	–	√
Cupples et al. [31]	–	H_2	–	DCE-VC	Monod kinetics (with biomass growth and decay)	–	Between DCE and VC	–	–	–	–	–	–	–
Cupples et al. [32]	–	H_2	–	PCE–TCE–DCE-VC	Monod kinetics (with biomass growth and decay)	–	Between chlorinated ethenes	-	–	–	–	–	–	–
Lee et al. [48]	Glucose	H_2 (from fermentation, butyrate and ethanol oxidation and formate)	√	PCE–DCE	Monod kinetics (with biomass growth and decay)	Methanogenesis	Between chloroethenes and between dechlorinators and methanogenators	–	√	–	–	–	–	–
Widdowson [107]	–	Fructose and sodium lactate	√	TCE–DCE–VC	Monod kinetics	Sulfate, iron and oxygen reduction	More chlorinated ethenes inhibit less chlorinated ethenes, self-inhibition	–	–	–	–	√	–	√
Yu and Semprini [115]	–	H_2, butanol	–	PCE/TCE–DCE-VC	Monod kinetics (with biomass growth and decay)	–	More chlorinated ethenes inhibit less chlorinated ethenes, self-inhibition	–	–	–	–	–	–	–
Amos et al. [4]	–	Acetate, H_2, pyruvate	√	PCE–TCE–DCE	Monod kinetics (with biomass growth and decay)	–	Between PCE and TCE, self-inhibition	–	–	–	√	√	–	–
Christ and Abriola [19]	Pentanol	H_2	√	PCE–TCE–DCE	Monod kinetics (with biomass growth and decay)	Methanogenesis or acetogenesis	Between DCE and VC	–	–	√	–	√	–	√

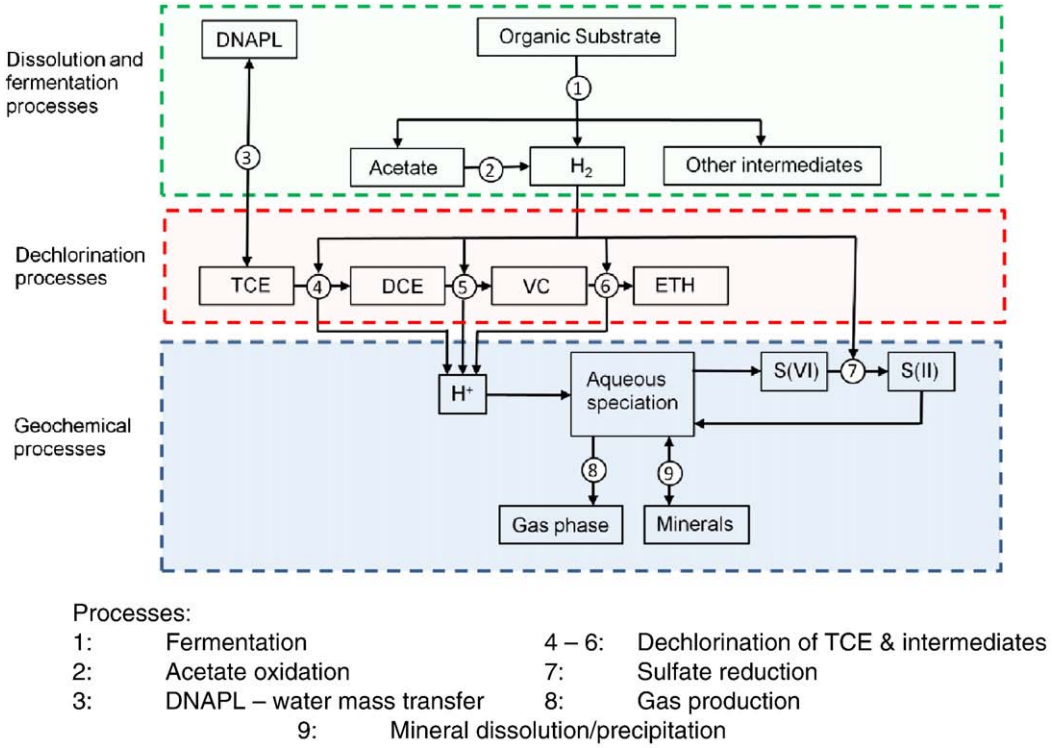

Fig. 1. Major processes and pathways involved in the anaerobic dechlorination of chlorinated ethenes. A description of the processes is provided in Section 2.

where C_{ps} [ML^{-3}] is the concentration of the primary substrate (ps) in the aqueous phase, t [T] is time, X_{FB} [$M_b L^{-3}$] is the biomass concentration for fermentative microbes (FB) and the subscript b in the units refers to biophase, k^{ps}_{max} [$M_c M_b^{-1} T^{-1}$] is the maximum utilization rate for primary substrate per unit fermentative biomass where the subscript c in the units refers to chemical species, K^{ps}_S [ML^{-3}] is the half-saturation constant for primary substrate, I_{Cl} is the competitive inhibition term, F (pH) is the pH inhibition function, C_{H_2S} [ML^{-3}] is the hydrogen sulfide (H_2S) aqueous concentration, $K_I^{H_2S}$ [ML^{-3}] is the hydrogen sulfide (H_2S) inhibition constant, and $\phi(H_2)$ is the H_2 inhibition function. The half-saturation constant (K^{ps}_S) in Eq. (17) is multiplied by an additional term (I_{Cl}) that accounts for inhibition of fermentation due to chloroethene toxicity [7]. This term is assumed to be equal to that for competitive inhibition between chloroethenes (see Eq. (25) and discussion below).

Inhibition of fermentation by H_2 may be important [36] and here it is represented by:

$$\phi(H_2) = \exp\left(-\frac{C_{H_2}}{C^{scale}_{H_2}}\right), \quad (18)$$

where C_{H_2} [ML^{-3}] is the aqueous concentration of H_2, and $C^{scale}_{H_2}$ [ML^{-3}] is the inhibitory aqueous concentration of H_2 for fermentation. Eq. (18) is a simplification (in the absence of the required/published data for $\Delta G°_{35\,°C}$) of the function suggested by Fennell and Gossett [36] to represent the distance of the fermentation reaction from thermodynamic equilibrium. A scale factor $C^{scale}_{H_2}$ is adopted instead of calculating the free energy; $C^{scale}_{H_2}$ represents the upper [H_2] threshold below which fermentation will proceed. Publications to date do not provide quantitative values for this threshold; rather they qualitatively suggest that, for example, both linoleic acid (vegetable oil emulsions) [84] and propionate [108] require a very low hydrogen partial pressure for fermentation to proceed. The value of $C^{scale}_{H_2}$ for linoleic acid in this work was obtained by calibration of the model to a series of 18 microcosm experiments using site soil and groundwater and varying TCE concentration, nutrient levels, degree of bioaugmentation, and other key variables (CL:AIRE bulletin on microcosm studies conducted within Source Area BioRemediation (SABRE) project ([40], http://www.claire.co.uk/sabre, http://www.claire.co.uk/library). The single $C^{scale}_{H_2}$ value was best-fit to the suite of experiments by optimizing the prediction of TCE, DCE, VC, and ETH concentration-time results (data not shown). If

Table 2
Stoichiometric representation of biological processes included in the conceptual model.

Process	Reaction	Eq.
Substrate fermentation (1)[a]	Substrate + $H_2O \rightarrow xH_2 + yCH_3COOH + zCO_2$ + intermediate products	(1)
Acetate oxidation (2)	$CH_3COOH + 2H_2O \rightarrow 4H_2 + 2CO_2$	(2)
DNAPL dissolution (3)	Chlorinated ethene (DNAPL) → Chlorinated ethene (aqueous phase)	(3)
Sequential degradation of chlorinated ethenes (4–6)	TCE → DCE, $H_2 + C_2HCl_3 \rightarrow H^+ + Cl^- + C_2H_2Cl_2$	(4)
	DCE → VC, $H_2 + C_2H_2Cl_2 \rightarrow H^+ + Cl^- + C_2H_3Cl$	(5)
	VC → ETH, $H_2 + C_2H_3Cl \rightarrow H^+ + Cl^- + C_2H_4$	(6)
Competing TEAPs	Sulfate reduction (7)	
	$SO_4^{2-} + 4H_2 \rightarrow H_2S + 2OH^- + 2H_2O$	(7)
	Iron reduction (9)	
	$2FeOOH + H_2 \rightarrow 2Fe^{2+} + 4OH^-$	(8)

[a]Notation corresponding to process number in Fig. 1.

Table 3
Stoichiometry of fermentation reactions for common organic substrates.

Organic substrate	Reaction	Eq.
Methanol[a]	$2CH_3OH \rightarrow CH_3COOH + 2H_2$	(9)
Ethanol[b]	$CH_3CH_2OH + H_2O \rightarrow CH_3COOH + 2H_2$	(10)
Lactate[b]	$CH_3CHOHCOOH + H_2O \rightarrow CH_3COOH + CO_2 + 2H_2$	(11)
Butyrate[b]	$CH_3CH_2CH_2COOH + 2H_2O \rightarrow 2CH_3COOH + 2H_2$	(12)
1-hexanol	$CH_3(CH_2)_4CH_2OH + 5H_2O \rightarrow 3CH_3COOH + 6H_2$	(13)
n-butyl-acetate	$CH_3COO(CH_2)_3CH_3 + 4H_2O \rightarrow 3CH_3COOH + H_2$	(14)
Glucose[c]	$C_6H_{12}O_6 + 2H_2O \rightarrow 2CH_3COOH + 2CO_2 + 4H_2$	(15)
Linoleic acid	$C_{18}H_{32}O_2 + 16H_2O \rightarrow 9CH_3COOH + 14H_2$	(16)

[a] [14].
[b] [36].
[c] [48].

C_{H_2} is low relative to the inhibitory $C_{H_2}^{scale}$ (i.e., the fermentation is far from equilibrium), the driving force for the fermentation reaction is high and $\phi(H_2)$ approaches 1. As the H_2 concentration approaches $C_{H_2}^{scale}$ (i.e., the reaction approaches equilibrium), the driving force is lessened.

Inhibition of fermentation by pH is well recognized [51,88] and several inhibition functions have been proposed [7,38,51]. Here the function of Bailey and Ollis [7] is employed:

$$F(\mathrm{pH}) = \left(1 + \frac{C_{H^+}}{K_1} + \frac{K_2}{C_{H^+}}\right)^{-1}, \tag{19}$$

where K_1 and K_2 [ML^{-3}] are the equilibrium constants for inactivation of the requisite enzyme by protonation and deprotonation, respectively, and C_{H^+} [ML^{-3}] is the proton concentration. This equation was chosen as it has been successfully applied to describe the inhibitory effect of pH on a reaction mediated by various anaerobic microbes, including methanogens and dechlorinators [117] and, in contrast to the equations of Fukuzaki et al. [38] and Lee et al. [51], is not limited to describing pH inhibition of fermentative microbes.

The last bracketed term in Eq. (17) comes into play in the presence of sulfide—the main product of sulfate reduction—which is a strong toxicant for many anaerobic microbes [46]. Sulfide toxicity is caused by its undissociated form H_2S, which can permeate cell membranes [81] and completely inhibit growth at concentrations around 550 mg L^{-1} free H_2S [45,62,68,80,98].

By individually calculating the values for substrate limitation (first bracketed quantity in Eq. (17)), and the pH, H_2 and sulfide inhibition terms, the rate-limiting term for fermentation can be determined. For instance, when the concentration of primary substrate C_{ps} is much higher than the value of the half-saturation constant K_S^{ps}, the term for primary substrate limitation will be close to 1, and will not limit the fermentation rate.

This model uses H_2 as the direct e-donor for TEAPs. Use of acetate as an e-donor is simulated by the oxidation of acetate to H_2 and CO_2 (process 2 in Fig. 1; [50]), typically occurring under low H_2 conditions [42,43]. A parameter, p, is used in the model to specify the fraction of acetate produced from substrate fermentation that breaks down according to Eq. (2) [84]. Hence, fermentation of an organic substrate is described in the model by two reactions. It is assumed that a proportion $(1-p)$ of fermentation proceeds via reactions that produce CH_3COOH and H_2, and the remainder (p) proceeds via reactions that produce the acetate breakdown products—CO_2 and H_2 [84]. Considering these reactions the production of H_2 by fermentors is given by:

$$\frac{dC_{H_2}}{dt} = (1-p)f_1\frac{dC_{ps}}{dt} + pf_2\frac{dC_{ps}}{dt}, \tag{20}$$

where f_1 and f_2 are stoichiometric coefficients of H_2 production in the fermentation reactions with and without acetate generated. Thus, for example, for linoleic acid $f_1 = 14$ and $f_2 = 50$, the first value is from Eq. (16) and the second from:

$$C_{18}H_{32}O_2 + 34H_2O \rightarrow 18CO_2 + 50H_2. \tag{21}$$

Studies have shown that acetate generated from substrate fermentation may serve as a direct e-donor for conversion of PCE and TCE to DCE, but not directly, if at all, in the conversion of DCE and VC [33,47,49,55,93,99]. Acetate can be utilized directly in denitrification, iron reduction, sulfate reduction [103,106] and acetoclastic methanogenesis [43,64]. However, to simplify parameterization of the kinetics of competing TEAPs and due to lack of information on parameter values associated with microbes using acetate as a direct electron donor, acetate is included in the model only as an indirect e-donor producing H_2. As homoacetogenesis [109,112] and methanogenesis [64] are often inhibited by low H_2 concentrations and high chlorinated solvent concentrations typically found in source zones these processes are expected to be negligible and therefore ignored in this model [109]. High chlorinated solvent concentrations are also inhibitory for acetoclastic methanogens [109] and as such this process is neglected. Oxygen and nitrate are generally reduced prior to the onset of dehalogenating conditions [72], and as this model only considers systems in their reduced dehalogenating state, these processes are also not considered in the model. In contrast, sulfate reduction (process 7 in Fig. 1) and iron reduction often occur concomitantly with dechlorination and thus in the model these electron acceptors compete with dechlorinators for H_2 [13,57].

Sulfate reduction rate is described by:

$$\frac{dC_{SO_4^{2-}}}{dt} = -k_{max}^{SO_4^{2-}} X_{SRB}\left(\frac{C_{SO_4^{2-}}}{K_S^{SO_4^{2-}} + C_{SO_4^{2-}}}\right) \times\left(\frac{C_{H_2} - C_{H_2}^{min}}{K_S^{H_2} + C_{H_2} - C_{H_2}^{min}}\right)F(\mathrm{pH})\left(1 - \frac{C_{H_2S}}{K_I^{H_2S}}\right)H\left(C_{H_2} - C_{H_2}^{min}\right), \tag{22}$$

where H is the Heaviside step function, $C_{SO_4^{2-}}$ [ML^{-3}] is the concentration of sulfate in the aqueous phase, X_{SRB} [M_bL^{-3}] is the biomass concentration for sulfate reducers (*SRB*), $k_{max}^{SO_4^{2-}}$ [$M_cM_b^{-1}T^{-1}$] is the maximum utilization rate for sulfate per unit sulfate-reducing biomass, $K_S^{SO_4^{2-}}$[ML^{-3}] is the half-saturation constant for sulfate, and $C_{H_2}^{min}$ [ML^{-3}] is the threshold H_2 aqueous concentration for sulfate reducers.

Iron reduction (Eq. (8) in Table 2) is incorporated into the model via the following equation for microbial reduction of solid phase Fe^{3+} iron oxide [85]:

$$R_{Fe^{3+}} = \left[Fe_{fss}^{3+}\right]V_{max}^{surf}\left(\frac{[FeB]_{ssn}}{K_{FeB} + [FeB]_{ssn}}\right)H\left(C_{H_2} - C_{H_2}^{min}\right), \tag{23}$$

where $R_{Fe^{3+}}$ [$ML^{-3}T^{-1}$] is the bulk rate of Fe^{3+} oxide reduction, $[Fe_{fss}^{3+}]$ [$M_{sites}L^{-3}$] is the bulk volumetric abundance of 'free' (i.e., microbially reducible) Fe^{3+} oxide surface sites, V_{max}^{surf} [$M(M_{sites})^{-1}L^{-3}T^{-1}$] is the maximum reduction rate constant dependent on iron-reducers (FeB) cell density, $[FeB]_{ssn}$ [cells $(M_{free\ surface\ sites})^{-1}$] is the surface site-normalized FeB cell density, and K_{FeB} [cells $(M_{free\ surface\ sites})^{-1}$] is the half-saturation constant for the relationship between FeB cell density and the iron oxide reduction rate constant.

The rate of dechlorination is described in the model by:

$$\frac{dC_i}{dt} = -k_{max}^i X_{bio}\left(\frac{C_i}{K_S^i I_{CI} + C_i I_{HI}}\right)\left(\frac{C_{H_2} - C_{H_2}^{min}}{K_S^{H_2} + C_{H_2} - C_{H_2}^{min}}\right)F(\mathrm{pH}) \times\left(1 - \frac{C_{H_2S}}{K_I^{H_2S}}\right)H\left(C_{H_2} - C_{H_2}^{min}\right), \tag{24}$$

$$I_{CI} = 1 + \frac{C_j}{K_I^j}, \tag{25}$$

$$I_{HI} = 1 + \frac{C_i}{K_{HI}^i}, \tag{26}$$

where subscripts i and j represent parent and daughter chlorinated ethenes, respectively, and C_i and C_j [ML^{-3}] are the aqueous concentrations of the parent and daughter chlorinated ethenes, $C_{H_2}^{min}$ [ML^{-3}] is the threshold aqueous concentration for H_2 for dechlorinators, X_{bio} [M_bL^{-3}] is the biomass concentration of the relevant dechlorinating population (X_{DC1} or X_{DC2}, details below), k_{max}^i [$M_cM_b^{-1}T^{-1}$] is the maximum specific utilization rate for chlorinated ethene i per unit dechlorinating biomass, K_S^i [ML^{-3}] is the half-saturation constant for chlorinated ethene i, $K_S^{H_2}$[ML^{-3}] is the half-saturation constant for H_2, I_{CI} is the competitive inhibition coefficient, K_I^j [ML^{-3}] is the competitive inhibition constant for

inhibiting chlorinated ethene j, I_{HI} is the Haldane inhibition term for chlorinated ethene i, and K^i_{HI} [ML^{-3}] is the Haldane inhibition constant.

In Eq. (24), the half-saturation constants for chlorinated ethenes (K^i_S) are multiplied by an additional term (I_{CI}) that accounts for the competitive inhibition between chlorinated ethenes for the dehalogenase active sites. The competitive inhibition constants (K^j_I in Eq. (25)) for each chlorinated ethene are assumed to be equal to the respective half-saturation constants (K^j_S) [114]. To simulate self-inhibition resulting from high chlorinated ethene concentration, Haldane inhibition [7] is included in Eq. (24) via I_{HI}. The Haldane inhibition term is given in Eq. (26).

In the model, two dechlorinating microbial populations are assumed: one capable of reducing TCE to DCE (*DC1*), and the other capable of reducing DCE via VC to ETH (*DC2*). This assumption is based on enrichment culture studies that suggested two distinct dechlorinating populations may be involved in transformation of TCE to ETH [30,87].

The growth and decay of biomass is described in the model as:

$$\frac{dX_{bio}}{dt} = -Y^i_{bio}\frac{dC_i}{dt} - k^{bio}_b X_{bio}, \tag{27}$$

where Y^i_{bio} [$M_b\,M_c^{-1}$] is the yield of biomass *bio* due to the reduction of component i, and k^{bio}_b [T^{-1}] is the first-order decay rate of the microbial population bio.

Concerning the relationship between microbial growth and groundwater flow, many models [20,23,29,101,102,104] have considered biomass clogging, i.e., porosity and thus permeability reduction due to biomass growth. Bioclogging is most likely to occur in the presence of aggressive nutrient injection. Since the present model focuses on the complexity of geochemical and biological interactions, bioclogging is not currently included.

In the model, equilibrium or rate-limited non-aqueous phase (NAP) dissolution is simulated (process 3 in Fig. 1). Rate-limited NAP dissolution is expressed as [89]:

$$\frac{dM_{NAP}}{dt} = -\gamma_i(C^e_i - C_i), \tag{28}$$

where M_{NAP} [ML^{-3}] is the total mass of NAP, C^e_i [ML^{-3}] is the concentration in the aqueous phase at equilibrium with NAP, C_i [ML^{-3}] is the concentration in the bulk aqueous phase; γ_i [T^{-1}] is the mass transfer rate coefficient for the NAP dissolution. Here, NAP and C_i are generic (i.e., not only for chlorinated ethenes; e.g., NAP could be DNAPL, vegetable oil or even gas). Various expressions have been developed for the calculation of γ (e.g., [39,44,65,69,75,76,88]). Each application of the model will require the most appropriate expression for γ to be implemented. In addition, transformation products can also partition back into NAP thus altering its composition [15,27] and partitioning is described in the model with the same linear driving force approach (Eq. (28)) but independent mass transfer coefficients are employed for NAP dissolution and for aqueous species back partitioning.

The processes discussed above influence the pH of the solution and, since many of the processes are acid-forming, the pH may reduce to levels that inhibit microbial activity. Acidity is generated directly from dechlorination (i.e., HCl) and also from the byproducts of e-donor fermentation. The acidity generated from fermentation depends on the specific e-donor used [63]. Furthermore, each TEAP competing with dechlorination increases the amount of e-donor fermented, and thus the acidity generated. The overall effects of the competing TEAPs on pH however are complicated because different amounts of alkalinity (OH^-) per mol of H_2 consumed are also added in the reduction reactions (Eqs. (7) and (8), [84]). The model explicitly simulates pH by accounting for all acidity and alkalinity contributing reactions and species; thus, the model allows for acidification by extensive microbial activity and the negative feedback this generates, while also allowing for the ability of the aqueous ions, minerals and gases present in the groundwater and soil to provide natural buffering to maintain the pH in an acceptable range for microbes.

The cation exchange capacity (CEC) of the soil may also contribute to a soil's natural buffering capacity as it releases cations while removing H^+ from solution. However, simulations conducted specifically to examine this issue indicate that the CEC only influences the buffering capacity when the pH drops below 4.5 because only then is the concentration of protons in the pore fluid comparable with that of other cations, and can therefore influence the equilibrium [84]. Since dechlorination, the focus of this model, is strongly inhibited at pH below 4.5 the CEC of the soil has been neglected.

pH is also influenced by the formation of a gas phase (process 8 in Fig.1), particularly if CO_2 is released. The release of CO_2(g) results in a decrease in CO_2(aq) and thus an increase in pH due to the shift in the dissolved carbonate equilibrium:

$$\frac{[H^+][HCO_3^-]}{[CO_2(aq)]} = K = 10^{-6.3}, \tag{29}$$

where K is the equilibrium constant and the bracketed quantities denote molar aqueous concentrations. Releasing CO_2 from the soil solution thus removes a mechanism for increasing H^+ concentrations. A gas phase is allowed to form in the model when the sum of all the partial pressures of the dissolved gases present in solution exceeds a specified total pressure. This total pressure corresponds to the hydrostatic pressure at a given depth below the water table.

The numerical model developed was implemented in PHREEQC version 2.15 [70]. The stoichiometric reactions (Eqs. (1), (2), (4)–(6), (16), (21)) and kinetic expressions (Eqs. (17), (20), (22)–(24), (27), and (28)) described above were added to the *minteq.v4* database [3] that is used by PHREEQC and otherwise contains all relevant equilibrium reactions and associated thermodynamic constants. The non-linear chemical equilibrium equations are solved by the Newton–Raphson method [70]. The kinetic reaction equations are ordinary differential equations that in PHREEQC are solved using CVODE [26], an implicit algorithm for stiff differential equations that includes internal time-step control [71]. The program has been demonstrated to be relatively robust and incorporates numerous options that are effective at ensuring convergence [71]. Simulation of sequential anaerobic dechlorination of tetrachloroethene (PCE) employing a first-order kinetic model was found to reproduce the analytical solution given by Beranger et al. [10] (Fig. A.1 in Supplementary Material). Analytical solutions are not available for verification of the complete model.

3. Numerical simulations

To explain the modeling approach and to illustrate the model's flexibility, several examples are presented. The model was first employed to simulate a batch system with conditions representative of a typical remediation site. Sensitivity analyses, both local and global, were then performed to determine the model parameters of most importance and the outcome sensitivity of coefficients used. Simulations described in Section 4 required from 0.08 to 1.7 h of computation time on Pentium workstations and number of Newton–Raphson iterations typically ranged from 85 to 145 before the Newton–Raphson method converged.

3.1. Base case simulation

For the base case (BC) simulation, the assumed initial solution and soil chemistry were based upon values representative of those measured for the Source Area BioRemediation (SABRE) site: a chemical manufacturing facility in the United Kingdom at which enhanced bioremediation research was conducted and thus extensive characterization of soil and groundwater has been undertaken

(Table 4, http://www.claire.co.uk/sabre). The base case TCE concentration was set to a high value (Table 4), representative of values observed within the DNAPL source zone at the site. The simulation employed linoleic acid ($C_{18}H_{32}O_2$) as the fermenting e-donor. This is a typical major component of commercial water-insoluble substrates containing vegetable oil (e.g., the soybean oil emulsion used at the SABRE site). It was assumed that excess linoleic acid was present as a free phase and in equilibrium with the solution (i.e., saturation index (SI) = 0). Dissolution of free phase linoleic acid was modeled as an equilibrium process (i.e., setting γ in Eq. (28) very high). Fermentation of linoleic acid produces H_2 and organic acids, such as acetate, lactate, propionate and butyrate. H_2 and acetate were included in the model as direct and indirect e-donors used for dechlorination, respectively. Lactate, propionate and butyrate were not included because: (i) their concentrations are typically significantly lower than acetate concentrations (CL:AIRE bulletin on SABRE column studies, http://www.claire.co.uk/library); (ii) they can ferment to acetate and H_2 [36]. Initial concentrations of microbes were assumed as given in Table 4. Further, it was specified that calcite was the only mineral present. The dissolution of calcite was taken as kinetically controlled [5]. The rate expression and constants used for calcite dissolution were based on the PHREEQC database [70].

All processes described in Section 2 were included in the base case simulation except gas release, Haldane inhibition, DNAPL dissolution, partitioning of the chlorinated ethenes into DNAPL, and microbial reduction of solid phase Fe^{3+}. The latter three processes were ignored because, for the sake of clarifying a base set of complex process interactions, DNAPL is absent in this scenario and it was decided to limit the competing TEAPs influencing dechlorination to one (here sulfate reduction). The effects of incorporating Haldane inhibition and gas release are explored in Sections 4.3 and 4.4, respectively.

Table 5 summarizes parameter values used in the base case simulation, most of which were average values obtained from the literature. Parameter values for linoleic acid utilizers were taken to be the same as for ethanol utilizers as reported by Fennell and Gossett [36], but with the specific maximum linoleic acid utilization rate adjusted downward from that at 35 °C to an 18 °C value assuming the rate was halved for each 10 °C decrease [7,82]. The same H_2 half-saturation constant was selected for both TCE and DCE/VC dechlorinators. Further assumed was that TCE and DCE/VC dechlorinators have the same H_2 threshold value, $C_{H_2}^{min}(DC1) = C_{H_2}^{min}(DC2)$ [108]. The H_2 threshold value for *SRB*, $C_{H_2}^{min}(SRB)$, was set equal to that for dechlorinators. Values for kinetic constants for the *SRB* were taken from Kalyuzhnyi et al. [46]. Other assumptions are indicated in Table 5. One exception to use of literature values was the value of the *SRB* hydrogen half-saturation constant ($K_S^{H_2}(SRB)$) because usage of the 1.1 μM value from Kalyuzhnyi et al. [46] resulted in insignificant sulfate reduction. This is not compatible with observations of significant sulfate reduction at the SABRE site. While the reason for the difference between the published and adopted [$K_S^{H_2}(SRB)$] values is not evident, there are several possible explanations: (i) different experimental conditions, such as e-donor (sucrose vs. emulsified vegetable oil in SABRE),

Table 4
Initial concentrations of aqueous components, microbial mass and minerals used for the base conditions.

Species	Concentration
TCE	5.0 mM
Ca	7.2 mM
Mg	2.3 mM
Na	5.9 mM
K	0.2 mM
S(+6)[a]	10.4 mM
Cl	0.2 mM
C(+4)	5.1 mM
Fermentative microbes (*FB*)	0.5 mg-protein L^{-1}
TCE dechlorinating microbes (*DC1*)	0.5 mg-protein L^{-1}
DCE/VC dechlorinating microbes (*DC2*)	1 mg-protein L^{-1}
Sulfate-reducing microbes (*SRB*)	0.5 mg-protein L^{-1}
Calcite ($CaCO_3$)	0.6 mol $kg\text{-}w^{-1}$
SRS	0.05 mol $kg\text{-}w^{-1}$
pH	6.97

[a] Notation showing redox state.

Table 5
Parameters used for the base conditions.

Parameters and units	Symbol	Value
Maximum utilization rates [μmol/mg-protein/day]		
Substrate reduction to H_2 by fermentors	k_{max}^{ps}	263[a,b]
TCE reduction to DCE by TCE dechlorinators	k_{max}^{TCE}	107[c]
DCE reduction to VC by DCE/VC dechlorinators	k_{max}^{DCE}	28[c]
VC reduction to ETH by DCE/VC dechlorinators	k_{max}^{VC}	19.5[c]
Maximum microbial population growth rate [day]		
Sulfate reducers	$\mu_{max}^{SO_4^{2-}}$	1.4[b,d]
Half-saturation constants [mol L^{-1}]		
Half-saturation constant for primary substrate	K_S^{ps}	17×10^{-6}[a]
Hydrogen half-saturation constant for dechlorinators	$K_S^{H_2}$ ($DC1$, $DC2$)	2×10^{-9}[e]
Hydrogen half-saturation constant for sulfate reducers	$K_S^{H_2}(SRB)$	2×10^{-7}[e]
Half-saturation constant for TCE	K_S^{TCE}	1.58×10^{-6}[f]
Half-saturation constant for DCE	K_S^{DCE}	2.16×10^{-6}[f]
Half-saturation constant for VC	K_S^{VC}	176.3×10^{-6}[c]
Half-saturation constant for sulfate reduction	$K_S^{SO_4^{2-}}$	200×10^{-6}[d]
Inhibition constants [mol L^{-1}]		
TCE competitive inhibition constant	K_I^{TCE}	1.58×10^{-6}[f,g]
DCE competitive inhibition constant	K_I^{DCE}	2.16×10^{-6}[f,g]
Hydrogen sulfide inhibition constant	$K_I^{H_2S}$	0.017[d]
Biomass yields [mg-protein/μmol of Cl^-]		
Yield of fermentors due to reduction of primary substrate	Y_{FB}^{ps}	0.00198[a]
Yield of TCE dechlorinators due to TCE reduction	Y_{DC1}^{TCE}	0.006[h]
Yield of DCE/VC dechlorinators due to DCE reduction	Y_{DC2}^{DCE}	0.006[h]
Yield of DCE/VC dechlorinators due to VC reduction	Y_{DC2}^{VC}	0.006[h]
Yield of sulfate reducers due to sulfate reduction	$Y_{SRB}^{SO_4^{2-}}$	0.0057[d]
First-order decay constants [day]		
First-order decay constant for fermentors	k_b^{FB}	0.024[a]
First-order decay constant for TCE dechlorinators	k_b^{DC1}	0.024[a]
First-order decay constant for DCE/VC dechlorinators	k_b^{DC2}	0.024[a]
First-order decay constant for sulfate reducers	k_b^{SRB}	0.06[d]
Threshold/maximum H_2 concentration [mol L^{-1}]		
Threshold H_2 concentration for TCE dechlorinators	$C_{H_2}^{min}$ ($DC1$)	2×10^{-9}[i]
Threshold H_2 concentration for DCE/VC dechlorinators	$C_{H_2}^{min}$($DC2$)	2×10^{-9}[i]
Threshold H_2 concentration for sulfate reducers	$C_{H_2}^{min}$ (SRB)	2×10^{-9}[j]
Inhibitory H_2 concentration for fermentative microbes	$C_{H_2}^{scale}(FB)$	8×10^{-9}[e]
Acetate usage coefficient [–]		
Fraction of acetate produced from donor fermentation that is subsequently used as an e-donor	p	0.5[e]
Equilibrium constants for pH inhibition function [mol L^{-1}]		
Equilibrium constant for enzyme inactivation by protonation	K_1	5.92×10^{-7}[k]
Equilibrium constant for enzyme inactivation by deprotonation	K_2	4.24×10^{-9}[k]

[a] [36].
[b] Adjusted to groundwater temperature of 18 °C.
[c] Assumed, but close to the average values from [36,41,48,117].
[d] [46].
[e] Value determined via calibration to SABRE microcosm experiments (unpublished).
[f] Average value for [36,41,48,117].
[g] As discussed in [117], inhibition constants are assumed to take the value of the appropriate half-saturation constant (e.g., $K_I^{TCE} = K_S^{TCE}$).
[h] [61].
[i] [111].
[j] Within the range of reported values: 1–15 nM [17,28,54,55,56].
[k] [117].

microbial competition (no competition between sulfate reduction and methanogenesis in SABRE) and soil mineralogy (higher concentrations of trace minerals in SABRE groundwater), and (ii) potentially different sulfate-reducing populations.

3.2. Local sensitivity simulations

An analysis was conducted of the relative local sensitivity of model outputs to changes in model parameters used in the base case. The local sensitivity (LS) analysis was based on Taylor series expansions. By varying a parameter β_n by a small increment, $\Delta\beta_n$, the model output of interest in the system:

$$O = O(\beta_1, \beta_2, \beta_3 \ldots \beta_m) \tag{30}$$

is given to first order by:

$$O(\beta_n + \Delta\beta_n) = O(\beta_n) + \frac{\partial O}{\partial \beta_n}\Delta\beta_n. \tag{31}$$

Thus, the sensitivity of the chosen model output to $\Delta\beta_n$ may be expressed as:

$$\varsigma_n = \frac{\partial O}{\partial \beta_n}. \tag{32}$$

In this study sensitivities were calculated using two-sided difference ratios as follows:

$$\varsigma_n = \frac{O(\beta_n + \Delta\beta_n) - O(\beta_n - \Delta\beta_n)}{2\Delta\beta_n}. \tag{33}$$

The sensitivities found indicate the relative importance of each parameter and can be used to rank them. The ranking based on relative sensitivity, ς_n, required parameters to be non-dimensionalized, which was accomplished as follows (e.g., [73]):

$$\sigma_n = \varsigma_n \frac{\beta_n}{O}. \tag{34}$$

Parameters for the batch base case were each independently changed by ±1%, ±2% and ±10% in Eq. (33), producing results that varied according to the degree of non-linearity of the model with respect to the specific parameter under consideration. A total of 210 local scale sensitivity simulations were performed. Two metrics were employed for the sensitivity analysis. The first metric, here called ethene metric, was the time required to reach a 98% ETH endpoint, i.e., the time required for 98% of the total chlorinated ethenes to be converted into ETH. For this evaluation, the molar chlorinated fraction, M_{CF}, was calculated based on the total moles, T, of each chlorinated ethene present in all phases as [40]:

$$M_{CF} = \frac{T_{TCE} + T_{DCE} + T_{VC}}{T_{TCE} + T_{DCE} + T_{VC} + T_{ETH}}, \tag{35}$$

where M_{CF} is unity at the beginning of a simulation when TCE is the only chlorinated species present and equals 0.02 with 98% converted to ETH. The second metric, here called chlorine metric, was the time required to reach a 98% Cl^- endpoint. In this case a normalized chlorine number, N_{Cl}, based on molar concentrations was used [40]:

$$N_{Cl} = \frac{3C_{TCE} + 2C_{DCE} + C_{VC}}{3(C_{TCE} + C_{DCE} + C_{VC} + C_{ETH})}. \tag{36}$$

The 98% Cl^- endpoint is reached when $N_{Cl} = 0.02$. The normalized chlorine number gives better resolution of the early progress of dechlorination prior to ETH production.

3.3. Global sensitivity simulations

Global sensitivity simulations were performed in order to explore the range of possible outcomes within the limits of published parameter values (or estimates of the limits when published values were unavailable). 18 global sensitivity simulations were conducted, and the results compared to the base case simulation (Table 6). The chlorine metric was used to analyze the results.

In case MonKin, sensitivity to the Monod kinetic parameters for chlorinated ethenes was explored. Each simulation employed a published set of Monod parameters determined from experiments with active dechlorinating populations in mixed cultures [36,48,114]. Variability in the reported Monod parameters may result from complicating factors such as: culture history, kinetic assay procedure and parameter correlation [52].

The aim of cases HydK(*DC*) and HydK(*SRB*) was to quantify the effect of the H_2 half-saturation constant ($K_s^{H_2}$) for dechlorinators and sulfate reducers, respectively, on the reductive dechlorination of TCE to ETH in a mixed consortium, where there is competition between hydrogen utilizing microorganisms. The half-saturation constants for H_2 utilizers indicate which microorganisms will out-compete others at different H_2 levels. In case HydK(*DC*), $K_s^{H_2}$ (*DC*1, *DC*2) was increased 7.5 times over the base case (from 2 nM to 15 nM) so that it corresponded to the minimum value reported in the literature [8,22]. In case HydK(SRB), the value of $K_s^{H_2}$ (*SRB*) used was reduced by one order of magnitude (from 200 nm to 20 nM). This was selected in order to explore the influence of increased competition for H_2, since published values for this parameter (e.g., $K_s^{H_2}$ (*SRB*) = 1100 nM [46]) result in negligible sulphate reduction in the base case system.

In case HydThres (*SRB*), two simulations were performed with different H_2 thresholds for sulfate reducers, representing different physiological consortia [53]. In HydThres(*SRB*)1, $C_{H_2}^{min}$(*SRB*) was 2 times lower (1 nM) and in HydThres(*SRB*)2 it was 7.5 times higher (15 nM) than in the base case (2 nM), covering the range of values reported by Löffler et al. [55].

Case Acet simulations were performed to examine the influence of acetate as an alternative e-donor on model results. In the absence of published data for p (the fraction of acetate produced from e-donor fermentation that is consumed for energy, Eq. (2)) four simulations were conducted to encompass its full range by setting $p = 0$ (no acetate consumed), 0.25, 0.75, and 1 (all acetate consumed), whereas in the base case $p = 0.5$.

Case InitTCE employed three simulations to examine the sensitivity of the model with respect to the initial TCE concentration, setting C_{TCE} equal to 0.2 times, 0.5 times, and 1.5 times the base case value (5 mM); this represents a range of 1–7.5 mM (saturated concentration equals 7.6 mM). InitTCE simulations investigated the influence of the different initial TCE concentrations on the competitive inhibition terms, I_{Cl} (Eq. (25)).

In case HaldInhib, Haldane inhibition associated with high chlorinated ethene concentrations was investigated. Although Eq. (24) contains both competitive and Haldane inhibition effects, for simplicity only competitive inhibition was incorporated in the base case. In the two HaldInhib simulations, Haldane inhibition constants reported by Yu and Semprini [115] for their cultures obtained from Evanite site in Corvallis, Oregon (EV; HaldInhib1) and Point Mugu Naval Weapon Facility, CA (PM; HaldInhib2) were included for comparison. The reported K_{HI} values for DCE and VC by the EV culture were an order of magnitude lower than those for the PM culture, while K_{HI} values reported for TCE were equal for both [115].

In case BufCap, the soil buffering capacity was neglected by setting the initial calcite concentration to zero, whereas in the base case calcite was initially present at 0.6 mol kg-w^{-1} (where kg-w stands

Table 6
Overview of the global sensitivity analysis simulations: Case-specific parameters/conditions used and the 98% Cl^- metric.

Case	Focus	Parameters/conditions varied with respect to base case (BC)						
		Symbol	Units	BC value	Sensitivity (S) value			
					MonKin1[a]	MonKin2[b]	MonKin3[c]	MonKin4[d]
MonKin	Monod kinetic parameters for chlorinated ethenes	k_{max}^{TCE}	[μmol/mg-protein/day]	107	72	366	125	124
		k_{max}^{DCE}	[μmol/mg-protein/day]	28	72	48	13.8	22
		k_{max}^{VC}	[μmol/mg-protein/day]	19.5	72	48	8.08	2.44
		K_s^{TCE}	[μmol L^{-1}]	1.58	0.54	1.4	1.8	2.76
		K_s^{DCE}	[μmol L^{-1}]	2.16	0.54	3.3	1.76	1.9
		K_s^{VC}	[μmol L^{-1}]	176.3	290	2.6	62.6	602
		K_I^{TCE}	[μmol L^{-1}]	1.58	0.54	1.4	1.8	2.76
		K_I^{DCE}	[μmol L^{-1}]	2.16	0.54	3.3	1.76	1.9
		Results			MonKin1	MonKin2	MonKin3	MonKin4
		Time, t_S [day], required to reach the 98% Cl^- endpoint			51.5	30.8	223	N/A[e]
		$\Delta t = t_s - t_{BC}$, [day]			−13.1	−33.8	+158.4	−[f]

Case	Focus	Parameters/conditions varied with respect to base case						
		Symbol	Units	BC value	Sensitivity value			
HydK(*DC*)	H_2 half-saturation constant for dechlorinators	$K_s^{H_2}$ (*DC*1, *DC*2)	[nmol L^{-1}]	2	15[g]			
		Results						
		Time, t_S [day], required to reach the 98% Cl^- endpoint			137.2			
		$\Delta t = t_s - t_{BC}$, [day]			+72.6			

Case	Focus	Parameters/conditions varied with respect to base case						
		Symbol	Units	BC value	Sensitivity value			
HydK(*SRB*)	H_2 half-saturation constant for sulfate−reducers	$K_s^{H_2}$ (*SRB*)	[nmol L^{-1}]	200	20			
		Results						
		Time, t_S [day], required to reach the 98% Cl^- endpoint			136.1			
		$\Delta t = t_s - t_{BC}$, [day]			+71.5			

Case	Focus	Parameters/conditions varied with respect to base case						
		Symbol	Units	BC value	Sensitivity value			
					HydThres(*SRB*)1	HydThres(*SRB*)2		
HydThres*(SRB)*	H_2 threshold concentration for sulfate reducers	$C_{H_2}^{min}$	[nmol L^{-1}]	2	1[h]	15[i]		
		Results			HydThres(*SRB*)1	HydThres(*SRB*)2		
		Time, t_S [day], required to reach the 98% Cl^- endpoint			65.0	63.6		
		$\Delta t = t_s - t_{BC}$, [day]			+0.6	−1.0		

Case	Focus	Parameters/conditions varied with respect to base case						
		Symbol	Units	BC value	Sensitivity value			
					Acet1	Acet2	Acet3	Acet4
Acet	Acetate breakdown	p	[–]	0.5	1	0.75	0.25	0
		Results			Acet1	Acet2	Acet3	Acet4
		Time, t_S [day], required to reach the 98% Cl^- endpoint			61.4	62.6	68.2	76.0
		$\Delta t = t_s - t_{BC}$, [day]			−3.2	−2.0	+3.6	+11.4

Case	Focus	Parameters/conditions varied with respect to base case					
		Symbol	Units	BC value	Sensitivity value		
					InitTCE1	InitTCE2	InitTCE3
InitTCE	Initial TCE concentration	C_{TCE}	[mmol L^{-1}]	5	1	2.5	7.5
		Results			InitTCE1	InitTCE2	InitTCE3
		Time, t_S [day], required to reach the 98% Cl^- endpoint			31.8	44.2	90.4
		$\Delta t = t_s - t_{BC}$, [day]			−32.8	−20.4	+25.8

(continued on next page)

Table 6 (*continued*)

Case	Focus	Parameters/conditions varied with respect to base case				
		Symbol	Units	BC value	Sensitivity value	
					HaldInhib1[j]	HaldInhib2[k]
HaldInhib	Haldane inhibition	K_{HI}^{TCE}	[μmol L^{-1}]	–	900	900
		K_{HI}^{DCE}	[μmol L^{-1}]	–	750	6000
		K_{HI}^{VC}	[μmol L^{-1}]	–	750	7000
		Results			HaldInhib1	HaldInhib2
		Time, t_S [day], required to reach the 98% Cl^- endpoint			NA	172.8
		$\Delta t = t_s - t_{BC}$, [day]			–	+108.2
Case	Focus	Parameters/conditions varied with respect to base case				
		Symbol	Units	BC value	Sensitivity value	
BufCap	Soil buffering capacity	M_{CaCO_3}	[mol kg-w^{-1}]	0.6	0	
		Results				
		Time, t_S [day], required to reach the 98% Cl^- endpoint			N/A	
		$\Delta t = t_s - t_{BC}$, [day]			–	

[a] Parameter values for case MonKin1 were taken from [36].
[b] Parameter values for case MonKin2 were taken from [48].
[c] Parameter values for case MonKin3 were taken from [117] and correspond to EV culture.
[d] Parameter values for case MonKin4 were taken from [117] and correspond to PM culture.
[e] Abbreviation NA indicates that 98% Cl^- endpoint was not reached within the simulation time of 350 d.
[f] A dash (–) indicates the value was not calculated or the parameter was not simulated in the subject case.
[g] Parameter value was taken from [8].
[h] Parameter value was set equal to the minimum from the range reported in [55].
[i] Parameter value was set equal to the maximum from the range reported in [55].
[j] Parameter values for case HaldInhib1 were taken from [115] and correspond to EV culture.
[k] Parameter values for case HaldInhib 2 were taken from [115] and correspond to PM culture.

for kg water). The purpose of the BufCap simulation was to evaluate the role of calcite in buffering the system.

3.4. Gas release simulations

The influence of gas release on the modeling results was examined by re-running the base case and three of the global sensitivity simulations (MonKin3, MonKin4, and BufCap) with the potential for gas to form included. In these simulations, a gas phase was allowed to form once the sum of the partial pressures of all gases produced exceeded 1.06 atm. This total pressure is equivalent to a location approximately 0.6 m below the water table, chosen arbitrarily. The initial partial pressures for all gases (H_2O, O_2, H_2S, NH_3, N_2, and H_2) were negligible except N_2 for which the partial pressure was set at 0.79 atm, and CO_2 for which the partial pressure was fixed by specifying the initial solution alkalinity and pH (Table 4). Global sensitivity cases MonKin3 and MonKin4 were chosen as examples representing standard situations (no extreme conditions, literature values for Monod kinetic parameters for chlorinated ethenes), whereas case BufCap was chosen because it was expected to be the case most susceptible to gas formation and therefore representing the results most affected by neglecting gas formation in the original sensitivity simulation (Case BufCap examined pH changes and pH is influenced by the formation of a gas phase (Eq. (29)).

4. Results

4.1. Base case simulation

For the base conditions the time required for complete degradation of chlorinated ethenes was found to depend strongly on the slower relative transformation kinetics for DCE and VC, compared with that for TCE (Fig. 2a). Here, k_{max}^{DCE} and k_{max}^{VC} are only one-fourth and one-fifth, respectively, of k_{max}^{TCE}. The K_s values are similar for DCE and TCE, but K_s^{VC} is approximately two orders of magnitude greater, further reducing the rate of VC transformation. The time needed to reach the 98% Cl^- endpoint (chlorine metric) was 65 days, whereas the time needed to reach the 98% ETH endpoint (ethene metric) was 66 days. Sulfate was the sole nonchlorinated electron accepter and its concentration was reduced from 10.4 mM to 8.7 mM over 100 days (Fig. 2b). The model predicted that after 14 days, when TCE dechlorination—the primary H_2 sink—was satisfied, H_2 increased sharply (Fig. 2c). Rapid increases in H_2 were also observed after 50 days and 67 days when DCE and VC dechlorination were complete, respectively. Although calcite was in excess, the resulting buffering capacity was not sufficient to maintain the pH above 6.5 (Fig. 2c). Calcite dissolution is limited by its solubility rather than by kinetic constraints [84], and only an inadequate 0.01 mol kg-w^{-1} of calcite was predicted to dissolve to help neutralize the 5 mM of HCl that resulted from dechlorination. The pH reduced to 6.2 by day 60, causing the rates of the microbial processes (fermentation, dechlorination, and sulfate reduction) to be reduced, although not stopped ($F(pH) = 0.6$).

4.2. Local sensitivity simulations

Fig. 3 shows the ranked importance of the top 13 of 35 parameters (in order of descending influence) based on the chlorine metric (Eq. (36)) and $\Delta\beta_n$ of 2%, while Table A.2 in the Supplementary Information provides the ranked importance of all the 35 parameters. A similar ranking was obtained based on the ETH metric (Eq. (35)). Using $\Delta\beta_n$ of 1%, 2% and 10% yielded identical ranking results for the top 8 parameters and nearly identical results for the other parameters (figures not shown). This indicates that the local sensitivity results are not strongly affected by non-linearities. Fig. 3 reveals that the maximum DCE utilization rate (k_{max}^{DCE}) and yield due to DCE degradation (Y_{DC2}^{DCE}) have the most significant influence on the time required for dechlorination. These two properties are followed in importance by the coefficient for pH inhibition by protonation (K_1), the maximum VC utilization rate (k_{max}^{VC}) and the first-order decay constant for DCE/VC dechlorinators (k_b^{DC2}). All of these parameters affect one key variable: the growth rate of

the DCE and VC dechlorinating population. For example, the maximum organism growth rate for DCE dechlorinators utilizing DCE equals $Y_{DC2}^{DCE} \cdot k_{max}^{DCE} - k_b^{DC2}$. Likewise, the protonation inhibition (Eq. (19)) directly acts to reduce growth rate as indicated in Eqs. (17) and (27). Significant here is that it is not the rate of dechlorination (k_{max}^{DCE}) by itself that is important in the time required to achieve 98% removal in the batch system, but it is the combined impact of all the factors affecting the overall growth rate.

Dechlorinators grow slowly, with a doubling time based upon the base line coefficients (Y_{bio}^{i}, k_{max}^{i}, k_b^{bio}) used for DCE dechlorinators of 4.8 days and for VC dechlorinators of 7.4 days. Fig. 2 indicates significant DCE dechlorination did not begin until after about 16 days, representing about 3.3 doubling times. Growth of VC dechlorinators could not begin until VC appearance at 16 days, after which about 34 days passed before significant VC dechlorination occurred, representing about 4.6 doublings. Four doublings would represent a population increase of 16 times that initially used. This indicates that had the initial population been assumed to be about 16 or more times larger, dechlorination of DCE and VC would have started almost immediately (assuming no lag effect). While in this sensitivity analysis the initial concentration of DCE/VC dechlorinators (X_{DC2}) seemed of less importance (seventh place ranking), in the field this value varies over orders of magnitude due to growth, decay, and possible bio-enhancement; thus its true impact is not captured as well in the limited range of variation used in this sensitivity analysis.

The ranking shown in Fig. 3 assists in better understanding how each parameter influences the model output; however, the results are specific to (i) the choice of sensitivity metrics, which here focus on complete degradation of chlorinated ethenes to non-hazardous ETH, and (ii) the parameter values selected, as well as the initial and boundary conditions of the chosen system. For the base case, based upon the startup of microcosms employing native SABRE site soil and groundwater, the time to reach 98% dechlorination was dominated by the growth rate of the DCE and VC dechlorinators relative to all other factors. However, this may not be true for other cases, such as during the steady-state operation of DNAPL dechlorination when relevant microbial populations are at peak, constant levels. For instance, while excess H_2 was available in this base case, it is expected that under H_2-limited conditions the H_2 half-saturation constants and the Monod kinetic parameters for fermentable e-donor will have a higher relative ranking.

4.3. Global sensitivity simulations

For case MonKin, investigating sensitivity to the kinetic parameters of published dechlorinating cultures, the obtained profiles for TCE, DCE, VC and ETH concentrations are shown in Fig. 4. In all cases, the organisms' yield and decay rates were assumed (in the absence of reported information in the key references employed) to be the same as in the base case; as a result, simulated differences in growth rates arose primarily due to differences in maximum utilization rates. As expected, the time scale associated with each chlorinated ethene in each plot in Fig. 4 (and Fig. 2 for base case) is clearly correlated to the magnitude of the maximum utilization rate of that species (Table 6). Table 6 summarizes the results of the chlorine metric relative to the base case. In case MonKin4 (PM culture, Yu [114]), the 98% Cl^- endpoint is never reached (Table 6), since the VC transformation rate decreased with time after DCE disappeared, reaching zero by approximately 150 days. Although this microbial population grew while dehalogenating DCE, its calculated growth rate is negative with only VC being dechlorinated. This suggests that the PM culture is similar to that of *Dehalococcoides ethenogenes strain 195*, which cometabolically transforms VC [116], thus indicating that it cannot grow on VC alone.

The results of increasing $K_s^{H_2}$ (*DC*1, *DC*2) in case HydK(*DC*) are presented in Fig. 5. As expected, such increases result in a decrease in growth rate, thus increasing the dechlorination time. Here, a 7.5-fold increase in $K_S^{H_2}$ (*DC*1, *DC*2) over the base case value increased the time to the 98% Cl^- endpoint to 137 days (~ twofold increase, compare Figs. 2a and 5a). The SO_4^{2-} (Fig. 5b), pH and H_2 (Fig. 5c) curves for HydK(*DC*) are identical to the base case curves apart from the timescale and the last H_2 peak. The peak in H_2 is lower in case HydK (*DC*) compared to the base case because the sulfate reducers consumed more H_2 with the longer time required for complete dechlorination to ETH. The half-saturation coefficient for H_2 utilization by sulfate reducers of 200 nM is an order of magnitude higher than the value used for dechlorinators, indicating that dechlorinators are expected to out-compete sulfate reducers for H_2 at low H_2 concentrations. It is noted, however, that for the conditions modeled there was no limitation on H_2 availability as there was insufficient H_2 demand (note: excess H_2 donor, linoleic acid, was assumed in the simulation).

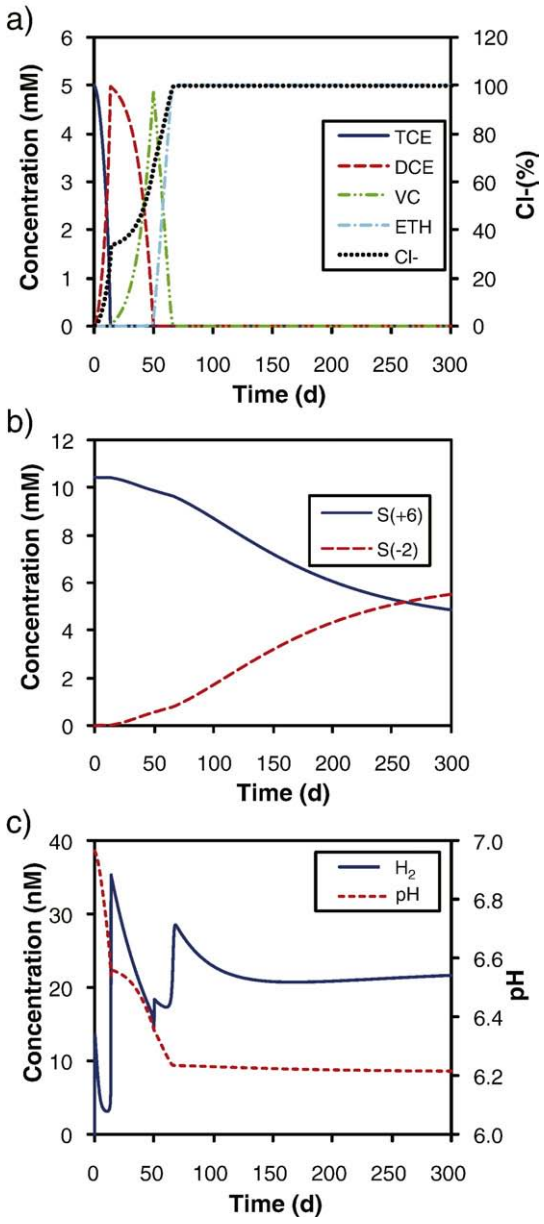

Fig. 2. Simulation results for the base conditions for (a) chlorinated ethenes concentrations; (b) sulfate and sulfide concentrations; and (c) H_2 concentrations and pH over time.

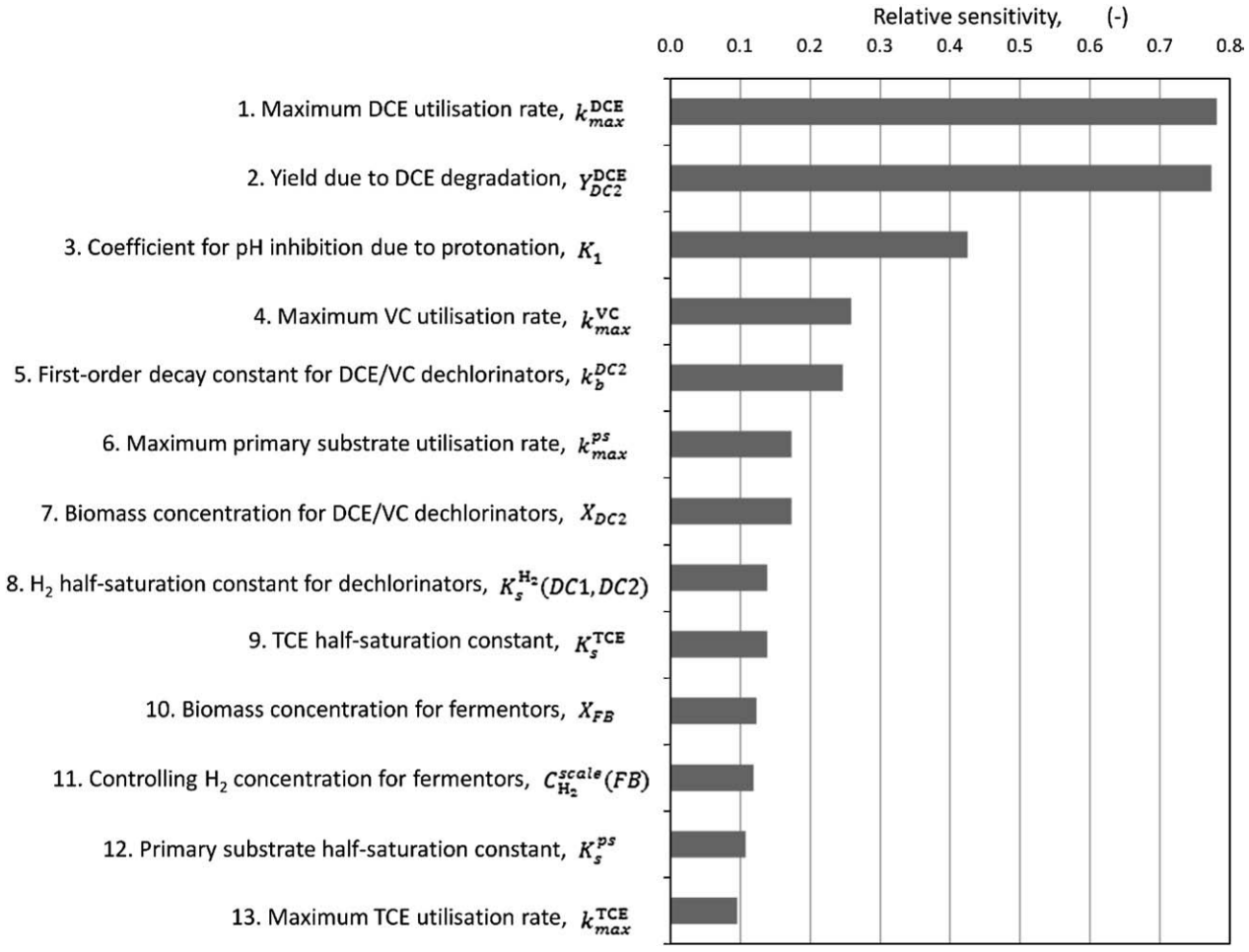

Fig. 3. Ranking of top 13 of 35 model parameters based on local sensitivity analysis.

Results for case HydK(*SRB*), examining the effect of reducing $K_S^{H_2}$ from 200 to 20 nM for sulfate-reducing microbes on dechlorination time, are presented in Fig. 6. Since decreasing $K_S^{H_2}(SRB)$ increases H_2 consumption by sulfate reducers, this leaves less H_2 available for dechlorinators and therefore the dechlorination rates decrease and the time to reach the 98% Cl^- endpoint increases. A 10-fold decrease in $K_S^{H_2}$ (*SRB*) increased the time to 136 days (~2-fold compared to the base case; Table 6). For case HydK(*SRB*), the H_2 level increased to 120 nM after all H_2 sinks were satisfied (Fig. 6c): first sulfate reduction (on day 35, Fig. 6b) and then dechlorination (on day 145).

The influence of H_2 threshold for sulfate reducers (case HydThres (*SRB*)) is presented in Table 6. The time required to reach 98% dechlorination was little different at 65 days for the base conditions with $C_{H_2}^{min}(SRB) = 1$ nM and 64 days when $C_{H_2}^{min}(SRB)$ equaled 15 nM. The effect of $C_{H_2}^{min}(SRB)$ on the dechlorination time is small compared to the other parameters examined. A H_2 threshold concentration of 1 nM is half the value used for dechlorinators, allowing sulfate reducers to out compete dechlorinators for hydrogen, while at 15 nM, the dechlorinators are favored. For this reason, less sulfate reduction occurred in the latter case (data not shown).

Results for case Acet, exploring model sensitivity to the degree to which acetate is utilized as an e-donor, are presented in Fig. 7 for the two endpoint simulations ($p = 1$ and $p = 0$). As expected, acetate utilization is beneficial for chlorinated ethene transformation: decreasing p (the fraction of acetate used) systematically increased the time required to reach the 98% Cl^- endpoint (up to a maximum increase of approximately 20% for $p = 0$, Table 6). Robinson et al. [84] demonstrated that acetate utilization also reduces the total e-donor requirement. The Acet simulation results agree with this: when $p = 1$, the predicted linoleic acid use was 6.4 mmol kg-w^{-1} for 98% dechlorination, but it increased to 7.2 mmol kg-w^{-1} with $p = 0$.

The effect of varying the initial TCE concentration between 1 and 7.5 mM was examined in case InitTCE. As expected, increasing TCE concentration increased the time to reach the 98% Cl^- endpoint (Table 6). For example, a 50% decrease of the initial TCE concentration relative to the base case value decreased the time to reach the 98% Cl^- endpoint to 44 d (32% decrease), whereas a 50% increase increased the time to 90 d (40% increase). The effect of competitive inhibition by chlorinated ethenes on the transformation of daughter products was also studied. As the TCE concentration was increased from 1 mM to 7.5 mM, the rate of VC production decreased, indicating that DCE dechlorination was inhibited by higher TCE concentrations. Inhibition of VC dechlorination by DCE was also observed. Fig. 8 illustrates the evolution of the TCE and DCE competitive inhibition terms (I_{Cl}, Eq. (25)) for different initial TCE concentrations; note that the higher the I_{Cl}, the higher the competitive inhibitory effect on microbial activity. As expected the inhibition coefficients peak when concentrations of the competing chlorinated ethene peaks and the magnitude of the peaks is approximately linearly related to the magnitude of the initial TCE concentration.

It is worth mentioning that if DNAPL is present in the system, it serves to deliver aqueous TCE concentrations at or near the solubility limit (depending on the mass transfer expression employed). Once DNAPL is depleted, the model predicts first very similar behavior to run

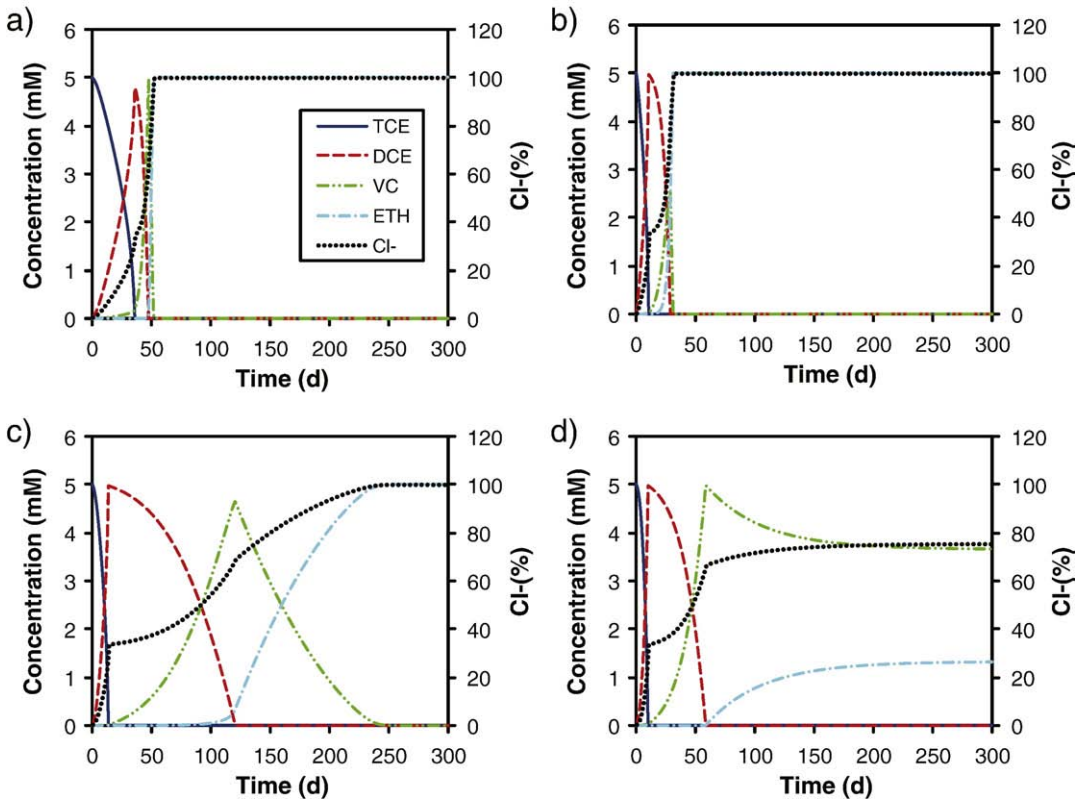

Fig. 4. Model-generated chlorinated ethenes concentration profiles over time based on Monod kinetic parameters from: (a) Fennell and Gossett [36] (MonKin1); (b) Lee et al. [48] (MonKin2); (c) Yu [117] for EV culture (MonKin3); (d) Yu [117] for PM culture (MonKin4). Legend in (a) refers to all subplots.

InitTCE3 ($C_{TCE} = 7.5$ mM) and then as TCE concentrations diminish, the predicted system behavior transitions to that for the other InitTCE runs. However, if the aqueous TCE concentration is at or near the solubility limit for an extended period of time (e.g., due to DNAPL presence), then the TCE inhibition term is constant and at maximum and the DCE inhibition term increases (until DCE solubility limit is reached) hindering dechlorination to VC and ETH (data not shown).

For case HaldInhib, the impact of including Haldane inhibition is shown in Fig. 9. Model simulations without (Fig. 2) and with Haldane inhibition (Fig. 9) yield considerably different results. In simulation HaldInhib1 (Fig. 9a) with the lowest Haldane coefficients, ETH was not produced, and only 33% of the base case Cl^- endpoint was reached after 60 d. In simulation HaldInhib2 with the higher coefficients, the time to reach a 98% ETH and Cl^- endpoints was almost 3 times longer than in the base case (Fig. 9b). This suggests that inclusion of Haldane kinetics is important when predicting reductive dechlorination of TCE at high concentrations. The Haldane coefficients used here as reported by Yu and Semprini [115] indicate that high DCE and VC concentrations are more toxic or inhibitory for the EV culture than for the PM culture, thus the toxicity appears to be culture specific.

Case BufCap examined the importance of soil buffering capacity. Fig. 10, where calcite is initially absent, indicates ETH was not produced, and only 28.4% of the base case Cl^- endpoint was reached after 100 days (Fig. 10a). The pH dropped to 4 within 100 days (Fig. 10b) and, therefore, microbially mediated dechlorination was severely inhibited. For comparison, when calcite was assumed to be initially present, the pH was predicted to drop to 6.2 after 100 days (Fig. 2d). Recall that the local sensitivity analysis showed that varying the base case initial amount of calcite $\pm 10\%$ had no impact (as expected, since calcite remained in excess). However, this underscores that calcite disappearance is clearly significant if no other alkalinity were present in the water to provide buffering capacity.

4.4. Possible gas release simulations

The model predicted that, for the base conditions simulated, the build-up of dissolved CO_2 accompanying dehalogenation leads to gas bubble formation at 59 days. This is when the partial pressure of all the gases sums to 1.06 atm. While N_2 is the dominant species when the gas phase forms (initial partial pressure = 0.79 atm), the gas composition changes as dehalogenation proceeds with the ratio of $CO_2(g)$ to $N_2(g)$ increasing (Supplementary Material, Fig. A.2). Despite this, for the base case, when a gas phase was permitted to form the time required to reach the 98% Cl^- endpoint was the same as when this process was neglected. There were no deviations in the key metrics for the local sensitivity simulations and conclusions remain unchanged. This is explained by the fact that the increase in $CO_2(g)$ concentrations were not sufficient to substantially alter the pH insofar as to affect the dechlorination rate in the examined system. Selected cases from the global simulations (MonKin3, MonKin4, and BufCap) were also tested assuming possible gas bubble formation. Observed deviations in time required to reach 98% Cl^- endpoint were not more than 4% compared to the respective simulations with no gas phase modeled (Supplementary Material, Fig. A.3). Note that even though gas release was modeled in the subset of simulations, its influence was limited to pH and other aqueous chemistry influences (i.e., pH may increase due to the shift in the carbonate equilibria as $CO_2(g)$ is released, Eq. (29), [84]). The influence of gas release on partitioning of chlorinated ethenes to the gas phase was not included in the model and as a result the impact of gas release may be underestimated. In addition, for simulations of

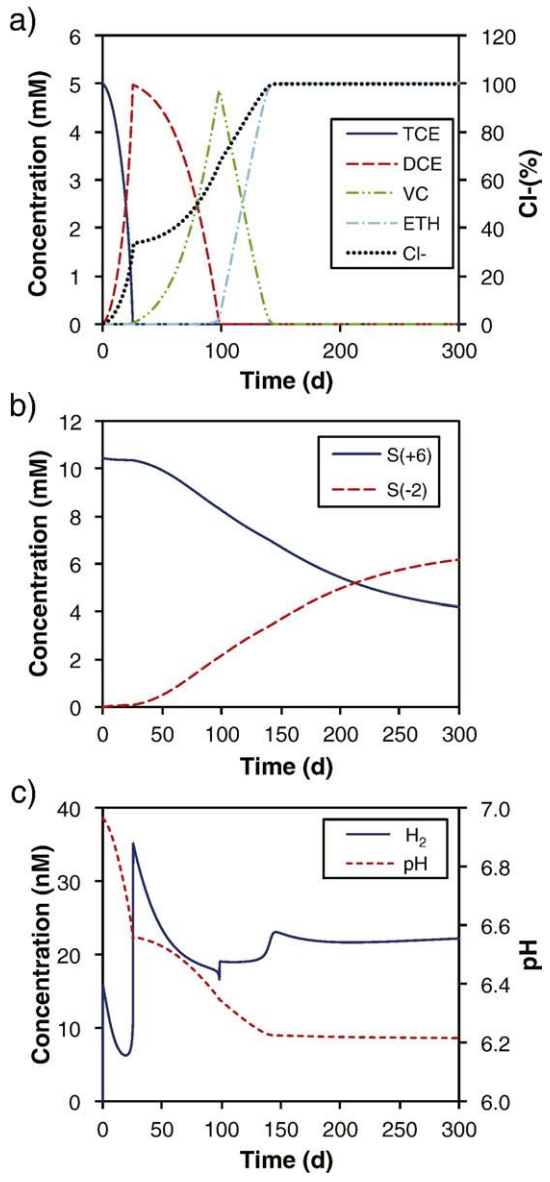

Fig. 5. Influence of H_2 half-saturation constant for dechlorinators, $K_S^{H_2}(DC1, DC2)$, on (a) chlorinated ethenes concentrations; (b) sulfate and sulfide concentrations; and (c) H_2 concentration and pH. Results are shown for the base conditions with $K_S^{H_2}(DC1, DC2) = 15$ nM (HydK(*DC*)).

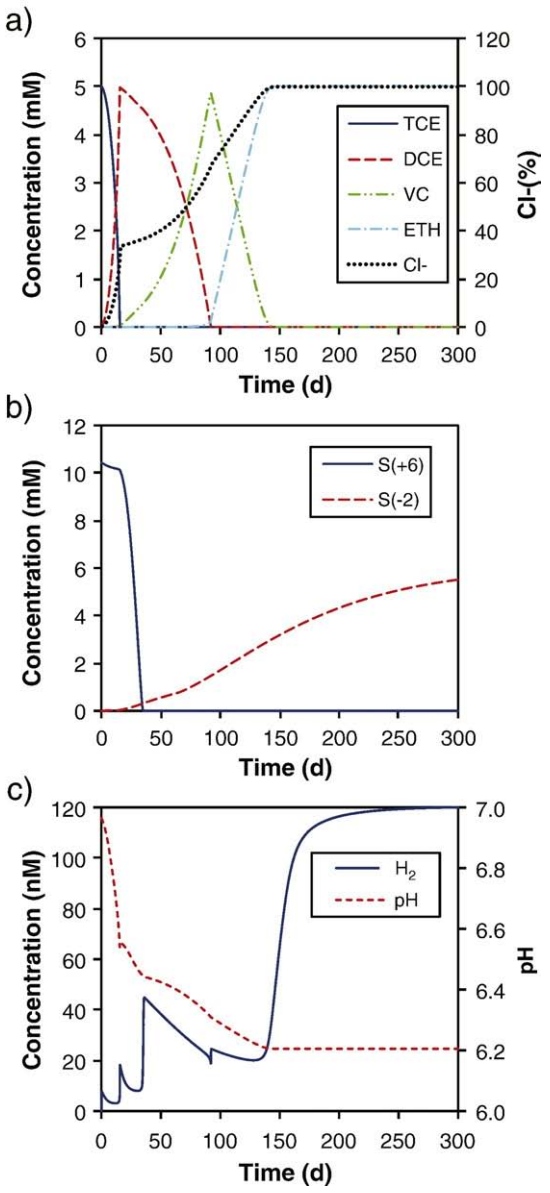

Fig. 6. Influence of H_2 half-saturation constant for sulfate reducers, $K_S^{H_2}(SRB)$, on (a) chlorinated ethenes concentrations; (b) sulfate and sulfide concentrations; (c) H_2 concentration and pH. Results are shown for the base conditions with $K_S^{H_2}(SRB) = 20$ nM.

flowing systems, gas production due to microbial activity and gas entrapment may result in reduced effective water permeability and flow diversion [111]. Therefore, the influence of gas release on permeability may be significant in such simulations.

5. Conclusions

A comprehensive approach for modeling enhanced biodegradation of chlorinated ethenes in DNAPL source zones has been developed. Simulations provide quantitative insight into the physical, chemical and biological processes involved, especially their interactions. The model developed considers site-water chemistry, mineral precipitation and dissolution, gas release, pH and alkalinity variations, free-phase DNAPL, aqueous phase chlorinated ethenes, e-donor, alternative terminal electron-accepting processes and microbial populations. The modeling examples presented in this work illustrated the ability of the model to simulate substrate fermentation, non-linear dechlorination kinetics (with competitor, product, and self-inhibition), growth and decay of four microbial populations, calcite precipitation/dissolution and pH feedback.

The sensitivity analysis indicated that DCE- and VC-related model parameters (i.e., k_{max}^{DCE}, Y_{DC2}^{DCE}, k_{max}^{VC}, k_b^{DC2}, X_{DC2}) are most critical to the model output. These all have impact on the maximum growth rate for the DCE and VC dechlorinating microorganisms, which in turn affects the time required for a small initial population to mature and attain sufficient concentrations to impact significantly the overall dechlorination rate of solvents. At high TCE concentrations, a significant competitive inhibitory effect is observed on the rates of microbial growth and efficiency of DCE and VC dechlorinating microorganisms, and this dominates the overall remediation times. Results suggest that this may be one reason why the reductive dechlorination of PCE and TCE at contaminated sites often results in the accumulation of DCE and VC (e.g., [60]), rather than ETH. The global sensitivity analysis further revealed pH control to be a crucial factor, as hydrochloric and organic acids are expected to accumulate in the source zone during bioremediation, leading to groundwater acidification and inhibitory

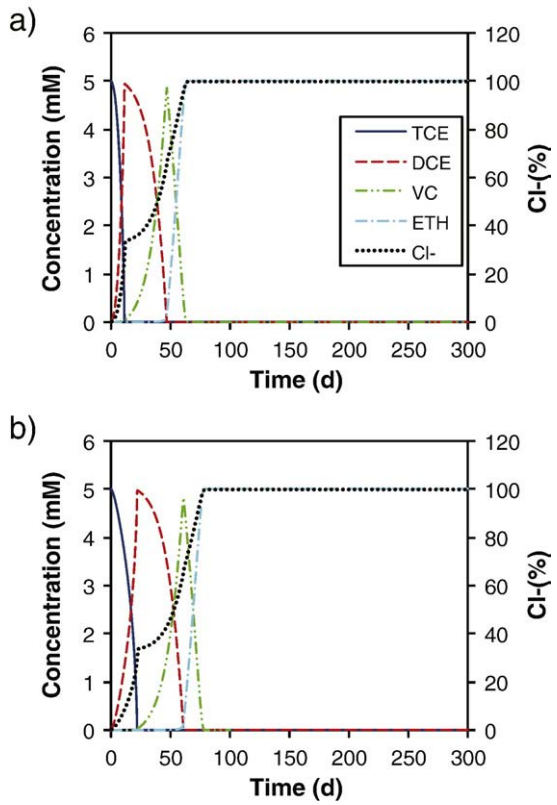

Fig. 7. Influence of acetate breakdown (p) on chlorinated ethenes concentrations. Results are shown for the base conditions with (a) $p=1.0$ (Acet1) and (b) $p=0$ (Acet4). The legend in (a) applies to both subplots.

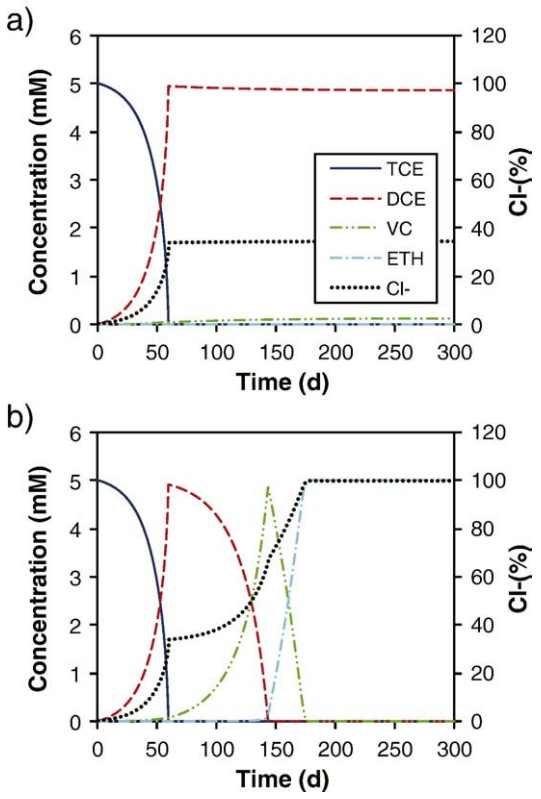

Fig. 9. Influence of incorporating Haldane inhibition on chlorinated ethenes concentrations. Results are shown for the base conditions with Haldane inhibition constants from Yu and Semprini [115] for (a) EV culture (HaldInhib1), and (b) PM culture (HaldInhib2). The legend in (a) applies to both subplots.

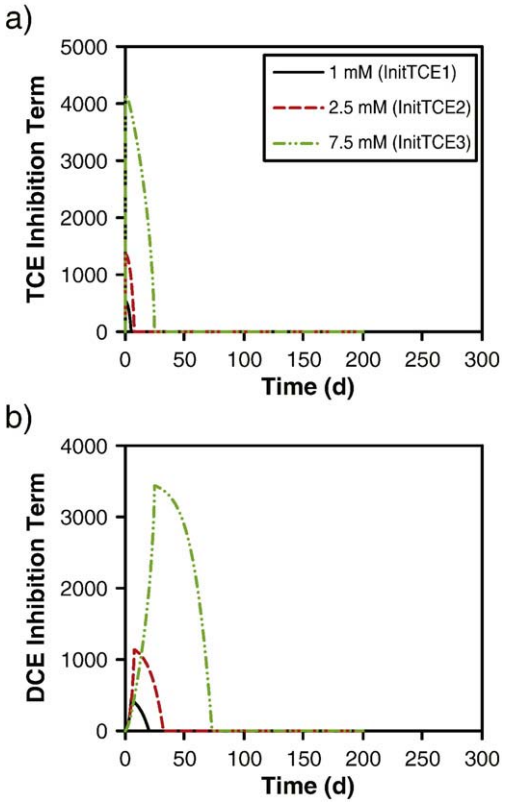

Fig. 8. (a) TCE and (b) DCE competitive inhibition term variation with time for different TCE initial concentrations. The legend in (a) applies to both subplots.

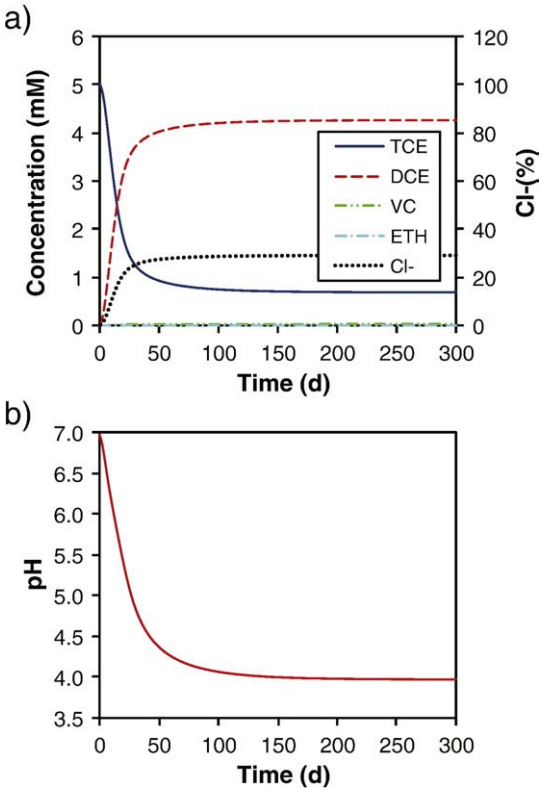

Fig. 10. Influence of soil buffering capacity (BufCap) on (a) concentrations of chlorinated ethenes, and (b) pH. Results are shown for the base conditions with calcite absent.

pH conditions for dehalogenating microorganisms. The soil buffering capacity may not be sufficient to prevent inhibitory acidic conditions alone, but for accurate predictions inclusion of the soil buffering capacity in a model is desirable as it has a significant impact. At high chlorinated solvent concentrations, inclusion of Haldane kinetics appears to also be important, however Haldane inhibition is culture specific [115]. Furthermore, the time required for dechlorination depends not only on dechlorination kinetics, but also on the kinetics of the competing nonchlorinated TEAPs. For instance, if sulfate reduction occurs, dechlorination is likely to proceed slower and more electron donor is likely to be required. Most of these conclusions reinforce ideas already known about the performance of these complex systems; indeed, it is the fact that the model produces a wide array of results that corroborate current understanding that provides confidence in its formulation and comprehensive inclusion of key processes.

This is the first model that explicitly accounts for reductive dechlorination by microbial communities as well as detailed soil–water geochemistry. As opposed to the recently developed biogeochemical models focused primarily on landfill leachate aquifer plumes, the presented model simulates parallel, rather than sequential, activity of multiple bacterial groups and their biochemical effects. The model proposed in this study requires validation through application to experimental data sets. For this purpose, data sets from the microcosm, column, and field studies conducted as part of the SABRE project (http://www.claire.co.uk/sabre) can be used. Since the computational expense of such comprehensive model is currently prohibitive for full field-scale applications, it is expected that the presented modeling approach is best employed as a tool to provide insight for understanding and optimizing bioremediation systems and to provide a benchmark for less complex but more practical field simulators.

Acknowledgements

This work was funded by BBSRC (BB/B519076/1) through the Bioremediation LINK Program, with additional support provided by Ecole Polytechnique Fédérale de Lausanne (EPFL, partially supported by SNF 200021_120160) and the University of Western Ontario (UWO). The authors acknowledge the industrial partners within the SABRE consortium—Acetate Products, Archon Environmental, British Geological Survey, Chevron, CL:AIRE, DuPont, Environment Agency (England and Wales), ESI, General Electric, GeoSyntec, Golder Associates, Honeywell, ICI, Scientifics, SiREM, Shell, Terra Systems, US EPA, DTI, EPSRC and NERC—whose contributions were critical to support the project. The authors thank Mark Harkness and other members of the laboratory and modeling teams within project SABRE for their advice on model development and illuminating data. The authors are also grateful to Alessandro Brovelli (EPFL) who provided advice on the cation exchange capacity of soils. Assistance in formatting the manuscript provided by Jessica Soo (UWO) is acknowledged.

Appendix A. Supplementary data

Supplementary data associated with this article can be found, in the online version, at doi:10.1016/j.advwatres.2010.04.017.

References

[1] Adamson DT, McDade JM, Hughes JB. Inoculation of a DNAPL source zone to initiate reductive dechlorination of PCE. Environ Sci Technol 2003;37(11):2525–33.
[2] Adamson DA, Lyon DY, Hughes JB. Flux and product distribution during biological treatment of tetrachloroethene dense non-aqueous-phase liquid. Environ Sci Technol 2004;38(7):2021–8.
[3] Allison J.D., Brown D.S., Novo-Gradac K.J. MINTEQA2/PRODEFA2—A geochemical assessment model for environmental systems—version 3.0 user's manual: Athens, Georgia, USA, Environmental Research Laboratory, Office of Research and Development, U.S. Environmental Protection Agency, 1990, 106 p.
[4] Amos BK, Christ JA, Abriola LM, Pennell KD, Loeffler FE. Experimental evaluation and mathematical modeling of microbially enhanced tetrachloroethene (PCE) dissolution. Environ Sci Technol 2007;41(3):963–70.
[5] Appelo CAJ, Postma D. Geochemistry, groundwater and pollution. 2nd ed. Amsterdam: A. A. Balkema Publishers; 2005. 649 pp.
[6] Bagley D. Systematic approach for modeling tetrachloroethene biodegradation. ASCE J Environ Eng 1998;124:1076–86.
[7] Bailey JE, Ollis DF. Biochemical engineering fundamentals. 2nd edition. New-York: McGraw-Hill; 1986.
[8] Ballapragada BS, Stensel HD, Puhakka JA, Ferguson JF. Effect of hydrogen on reductive dechlorination of chlorinated ethenes. Environ Sci Technol 1997;31(15):1728–34.
[9] Barry DA, Prommer H, Miller CT, Engesgaard P, Brun A, Zheng C. Modelling the fate of oxidisable organic contaminants in groundwater. Adv Water Resour 2002;25(8–12):945–83.
[10] Beranger SC, Sleep BE, Lollar BS, Monteagudo FP. Transport, biodegradation and isotopic fractionation of chlorinated ethenes: modelling and parameter estimation methods. Adv Water Resour 2005;28:87–98.
[11] Brun A, Engesgaard P. Modelling of transport and biogeochemical processes in pollution plumes: literature review and model development. J Hydrol 2002;256:211–27.
[12] Brun A, Engesgaard P, Christensen TH, Rosbjerg D. Modelling of transport and biogeochemical processes in pollution plumes: Vejen landfill, Denmark. J Hydrol 2002;256:228–47.
[13] Caccavo F, Blakemore RP, Lovley DR. A hydrogen-oxidizing, Fe(III)-reducing microorganism from the Great Bay Estuary, New Hampshire. Appl Environ Microbiol 1992;58(10):3211–6.
[14] Carr CS, Hughes JB. Enrichment of high rate PCE dechlorination and comparative study of lactate, methanol, and hydrogen as electron donors to sustain activity. Environ Sci Technol 1998;32(12):1817–24.
[15] Carr CS, Garg S, Hughes JB. Effect of dechlorinating bacteria on the longevity and composition of PCE-containing nonaqueous phase liquids under equilibrium dissolution conditions. Environ Sci Technol 2000;34(6):1088–94.
[16] Chapelle FH. Identifying redox conditions that favor natural attenuation of chlorinated solvents in contaminated ground-water systems. Proceedings of the Symposium on Natural Attenuation of Chlorinated Organics in Ground Water, Dallas, Texas, EPA/540/R-96/509; 1996.
[17] Chapelle FH, Haack SK, Adriaens P, Henry MA, Bradley PM. Comparison of Eh and H_2 measurements for delineating redox processes in a contaminated aquifer. Environ Sci Technol 1996;30(12):3565–9.
[18] Christ JA, Ramsburg CA, Abriola LM, Pennell KD, Löffler FE. Coupling aggressive mass removal with microbial reductive chlorination for remediation of DNAPL source zones: a review and assessment. Environ Health Perspect 2005;113(4):465–74.
[19] Christ JA, Abriola LM. Modeling metabolic reductive dechlorination in dense non-aqueous phase liquid source-zones. Adv Water Resour 2007;30(6–7):1547–61.
[20] Chu M, Kitanidis PK, McCarty PL. Effects of biomass accumulation on microbially enhanced dissolution of a PCE pool: a numerical simulation. J Contam Hydrol 2003;65(1–2):79–100.
[21] Chu M, Kitanidis PK, McCarty PL. Possible factors controlling the effectiveness of bioenhanced dissolution of non-aqueous phase tetrachloroethene. Adv Water Resour 2004;27(6):601–15.
[22] Clapp LW, Semmens MJ, Novak PJ, Hozalski RM. Model for in situ perchloroethene dechlorination via membrane-delivered hydrogen. ASCE J Environ Eng 2004;130(11):1367–81.
[23] Clement TP, Hooker BS, Skeen RS. Macroscopic models for predicting changes in saturated porous media properties caused by microbial growth. Ground Water 1996;34(5):934–42.
[24] Clement TP. A modular computer code for simulating reactive multispecies transport in 3-dimensional groundwater systems. Technical Report PNNL-SA-11720. Richland, Washington: Pacific Northwest National Laboratory; 1997.
[25] Clement TP, Johnson CD, Sun YW, Klecka GM, Bartlett C. Natural attenuation of chlorinated ethene compounds: model development and field-scale application at the Dover site. J Contam Hydrol 2000;42(2–4):113–40.
[26] Cohen SD, Hindemarsh AC. CVODE, a stiff/nonstiff ODE solver. C: Computers in Physics, vol. 10,(2); 1996. p. 138.
[27] Cope N, Hughes JB. Biologically-enhanced removal of PCE from NAPL source zone. Environ Sci Technol 2001;35(10):2014–21.
[28] Cord-Ruwisch R, Seitz H-J, Conrad R. The capacity of hydrogenotrophic anaerobic bacteria to compete for traces of hydrogen depends on the redox potential of the terminal electron acceptor. Arch Microbiol 1988;149:350–7.
[29] Cunningham AB, Characklis WG, Abedeen F, Crawford D. Influence of biofilm accumulation on porous medium hydrodynamics. Environ Sci Technol 1991;25(7):1305–11.
[30] Cupples AM, Spormann AM, McCarty PL. Growth of Dehalococcoides-like microorganism on vinyl chloride and cis-dichloroethene as electron acceptors as determined by competitive PCR. Appl Environ Microbiol 2003;69(7):953–9.
[31] Cupples AM, Spormann AM, McCarty PL. Vinyl chloride and cis-dichloroethene dechlorination kinetics and microorganism growth under substrate limiting conditions. Environ Sci Technol 2004;38(6):1102–7.
[32] Cupples AM, Spormann AM, McCarty PL. Comparative evaluation of chloroethene dechlorination to ethene by *dehalococcoides*-like microorganisms. Environ Sci Technol 2004;38(18):4768–74.

[33] Dolfing J, Tiedje JM. Acetate as a source of reducing equivalents in the reductive dechlorination of 2, 5-dichlorobenzoate. Arch Microbiol 1991;156(5):356–61.
[34] Duhamel M, Wehr SD, Yu L, Rizvi H, Seepersad D, Dworatzek S, Cox EE, Edwards EA. Comparison of anaerobic dechlorinating enrichment cultures maintained on tetrachloroethene, trichloroethene, cis-dichloroethene and vinyl chloride. Water Res 2002;36(17):4193–202.
[35] Ellis DE, Lutz EJ, Odom JM, Buchanan Jr RJ, Bartlett CL, Lee MD, Harkness MR, Deweerd KA. Bioaugmentation for accelerated in situ anaerobic bioremediation. Environ Sci Technol 2000;34(11):2254–60.
[36] Fennell DE, Gossett JM. Modeling the production of and competition for hydrogen in a dechlorinating culture. Environ Sci Technol 1998;32(16):2450–60.
[37] Fennell DE, Gossett JM, Zinder SH. Comparison of butyric acid, ethanol, lactic acid, and propionic acid as hydrogen donors for the reductive dechlorination of tetrachloroethene. Environ Sci Technol 1997;31(3):918–26.
[38] Fukuzaki S, Nishio N, Shobayashi M, Nagai S. Inhibition of the fermentation of propionate to methane by hydrogen, acetate, and propionate. Appl Environ Microbiol 1990;56(3):719–23.
[39] Geller JT, Hunt JR. Mass transfer from nonaqueous phase organic liquids in water-saturated porous media. Water Resour Res 1993;29(4):833–45.
[40] Harkness M, Fisher A, Lee M, Mack EE, Payene JA, Roberts J, Dworatzek S, Possolo A, Acheson C. Reductive dechlorination of high levels of TCE in a multi-lab, statistically-based microcosm study. *In preparation 2010*.
[41] Haston ZC, McCarty PL. Chlorinated ethene half-velocity coefficients (K_S) for reductive dehalogenation. Environ Sci Technol 1999;33(2):223–6.
[42] He J, Sung Y, Dollhope ME, Fathepure BZ, Tiedje JM, Loffler FE. Acetate versus hydrogen as direct electron donors to stimulate the microbial reductive dechlorination process at chloroethene-contaminated sites. Environ Sci Technol 2002;36(18):3945–52.
[43] Heimann AC, Batstone DJ, Jakobsen R. Methanosarcina spp. drive vinyl chloride dechlorination via interspecies hydrogen transfer. Appl Environ Microbiol 2006;72(4):2942–9.
[44] Imhoff PT, Jaffé PR, Pinder GF. An experimental study of complete dissolution of a nonaqueous phase liquid in saturated porous media. Water Resour Res 1993;30(2):307–20.
[45] Kalyuzhnyi S, de Leon Fragaso C, Rodriguez Martinez J. Biological sulphate reduction in an UASB reactor fed with ethanol as electron donor. Mikrobiologiya 1997;66(5):562–7.
[46] Kalyuzhnyi S, Fedorovich V, Lens P, Pol LH, Lettinga G. Mathematical modelling as a tool to study population dynamics between sulphate reducing and methanogenic bacteria. Biodegradation 1998;9(3–4):187–99.
[47] Krumholz LR, Sharp R, Fishbain SS. A freshwater anaerobe coupling acetate oxidation to tetrachloroethylene dehalogenation. Appl Environ Microbiol 1996;62(11):4108–13.
[48] Lee IS, Bae J-H, Yang Y, McCarty PL. Simulated and experimental evaluation of factors affecting the rate and extent of reductive dehalogenation of chloroethenes with glucose. J Contam Hydrol 2004;74(1–4):313–31.
[49] Lee IS, Bae JH, McCarty PL. Comparison between acetate and hydrogen as electron donors and implications for the reductive dehalogenation of PCE and TCE. J Contam Hydrol 2007;94(1–2):76–85.
[50] Lee MJ, Zinder SH. Isolation and characterization of a thermophilic bacterium which oxidizes acetate in syntrophic association with a methanogen and which grows acetogenically on H_2–CO_2. Appl Environ Microbiol 1988;54(1):124–9.
[51] Lee YJ, Miyahara T, Noike T. Effect of pH on microbial hydrogen fermentation. J Chem Technol Biotechnol 2002;77(6):694–8.
[52] Liu C, Zachara JM. Uncertainties of Monod kinetic parameters nonlinearly estimated from batch experiments. Environ Sci Technol 2001;35(1):133–41.
[53] Lovley DR, Goodwin S. Hydrogen concentrations as an indicator of the predominant terminal-accepting reactions in aquatic sediments. Geochim Cosmochim Acta 1988;52(12):2993–3003.
[54] Lowe SE, Jain MK, Zeikus JG. Biology, ecology, and biotechnical applications of anaerobic bacteria adapted to environmental stresses in temperature, pH, salinity, or substrates. Microbiol Rev 1993;57:451–509.
[55] Löffler FE, Tiedje JM, Sanford RA. Fraction of electrons consumed in electron acceptor reduction and hydrogen thresholds as indicators of halorespiratory physiology. Appl Environ Microbiol 1999;65(9):4049–56.
[56] Lu X, Tao S, Bosma T, Gerritse J. Characteristic hydrogen concentrations for various redox processes in batch study. J Environ Sci Health 2001;A36(9):1725–34.
[57] Luijten MLGC, Roelofsen W, Langenhoff AAM, Schraa G, Stams AJM. Hydrogen threshold concentrations in pure cultures of halorespiring bacteria and at a site polluted with chlorinated ethenes. Environ Microbiol 2004;6(6):646–50.
[58] Maillard J, Schumacher W, Vazquez F, Regeard C, Hagen WR, Hollinger C. Characterization of the corrinoid iron–sulfur protein tetrachloroethene reductive dehalogenase of *Dehalobacter restrictus*. Appl Environ Microbiol 2003;69(8):4628–38.
[59] Major D. Accelerated bioremediation of chlorinated solvents: principles and practices. Presentation in: a NATO-sponsored Advanced Study Institute in Prague, Czech Republic; 2001. See: http://www.hsrc.org/prague/major/slide40.html.
[60] Major DW, McMaster ML, Cox EE, Edwards EA, Dworatzek SM, Hendrickson ER, Starr MG, Payne JA, Buonamici LW. Field demonstration of successful bioaugmentation to achieve dechlorination of tetrachloroethene to ethene. Environ Sci Technol 2002;36(23):5106–16.
[61] Maymo-Gatell X, Chien YT, Gossett JM, Pol LH, Lettinga G. Isolation of bacterium that reductively dechlorinates tetrachloroethene to ethene. Science 1997;276(5318):1568–71.
[62] McCartney DP, Oleszkiewicz JA. Sulfide inhibition of anaerobic degradation of lactate and acetate. Water Res 1991;25(2):203–9.
[63] McCarty PL, Chu MY, Kitanidis PK. Electron donor and pH relationships for biologically enhanced dissolution of chlorinated solvent DNAPL in groundwater. Euro J Soil Biol 2007;43(5–6):276–82.
[64] McGuire JT, Smith EW, Long DT, Hyndman DW, Haack SK, Klug MJ, Velbel MA. Temporal variations in parameters reflecting terminal-electron-accepting processes in an aquifer contaminated with waste fuel and chlorinated solvents. Chem Geol 2000;169(3–4):471–85.
[65] Miller CT, Poirier-McNeill MM, Mayer AS. Dissolution of trapped nonaqueous phase liquids: mass transfer characteristics. Water Resour Res 1990;26(11):2783–96.
[66] Murphy EM, Ginn TR. Modeling microbial processes in porous media. Hydrogeol J 2000;8(1):142–58.
[67] Nielsen RB, Keasling JD. Reductive dechlorination of chlorinated ethene DNAPLs by a culture enriched from contaminated groundwater. Biotechnol Bioeng 1999;62(2):160–5.
[68] Okabe S, Nielsen PH, Characklis WG. Factors affecting sulfate reduction by *Desulfovibrio desulfuricans* in continuous culture: limiting nutrients and sulfide concentration. Biotechnol Bioeng 1992;40(6):725–34.
[69] Parker JC, Katyal AK, Kaluarachchi JJ, Lenhard RJ, Johnson TJ, Jayaraman K, Unlu K, Zhu JL. Modeling multiphase organic chemical transport in soils and ground water. Rep. EPA/600/2–91/042, U.S. Environmental Protection Agency, Washington, D.C; 1991.
[70] Parkhurst DL, Appelo CAJ. User's Guide to PHREEQC—a computer program for speciation, reaction-path, 1D-transport, and inverse geochemical calculations. Technical Report 99-4259. USA: U.S. Geological Survey; 1999.
[71] Parkhurst DL, Kipp KL, Engesgaard P, Charlton SR. PHAST—a program for simulating ground-water flow, solute transport, and multicomponent geochemical reactions: U.S. Geological Survey Techniques and Methods 6-A8; 2004. 154 pp.
[72] Parsons Corporation. Principles and practices of enhanced anaerobic bioremediation of chlorinated solvents. Prepared for: Air Force Center for Environmental Excellence, Brooks City-Base, Texas, Naval Facilities Engineering Service Center, Port Hueneme, California and Environmental Security Technology Certification Program, Arlington, Virginia, 2004.
[73] Pastres R, Ciavatta S. A comparison between the uncertainties in model parameters and in forcing functions: its application to a 3D water-quality model. Environ Mod Soft 2005;20(8):981–9.
[74] Powers SE, Loureiro CO, Abriola LM, Weber Jr WJ. Theoretical study of the significance of nonequilibrium dissolution of nonaqueous phase liquids in subsurface systems. Water Resour Res 1991;27(4):463–77.
[75] Powers SE, Abriola LM, Weber Jr WJ. An experimental investigation of nonaqueous phase liquid dissolution in saturated subsurface systems: steady-state mass transfer rates. Water Resour Res 1992;28(10):2691–705.
[76] Powers SE, Abriola LM, Weber Jr WJ. An experimental investigation of nonaqueous phase liquid dissolution in saturated subsurface systems: transient mass transfer rates. Water Resour Res 1994;30(2):321–32.
[77] Prommer H, Barry DA, Davis G. A one-dimensional reactive multi-component transport model for biodegradation of petroleum hydrocarbons in groundwater. Environ Mod Soft 1999;14(2–3):213–23.
[78] Prommer H, Barry DA, Zheng C. PHT3D—a MODFLOW/MT3DMS based reactive multi-component transport model. Ground Water 2003;42(2):247–57.
[79] Prommer H, Barry DA, Davis G. Modelling of physical and reactive processes during biodegradation of a hydrocarbon plume under transient groundwater flow conditions. J Contam Hydrol 2002;59(1–2):113–31.
[80] Reis MAM, Almeida JS, Lemos PC, Carrondo MJT. Effect of hydrogen sulfide on growth of sulfate-reducing bacteria. Biotechnol Bioeng 1992;40(5):593–600.
[81] Rinzema A. Anaerobic treatment of wastewater with high concentration of lipids and sulphate. PhD thesis, Wageningen Agricultural University, The Netherlands, 1988.
[82] Ristow NE, Hansford GS. Modelling of a falling sludge bed reactor using AQUASIM. Water SA 2001;27(4):445–54.
[83] Rittmann BE, Seagren E, Wrenn BA. In-situ bioremediation. 2nd ed. Parkridge, NJ: Noyes Publications; 1994. pp. 37–50.
[84] Robinson C, Barry DA, McCarty PL, Gerhard JI, Kouznetsova I. pH control for enhanced reductive source zone bioremediation of chlorinated solvents. Sci Total Environ 2009;407(16):4560–73.
[85] Roden EE. Geochemical and microbiological controls on dissimilatory iron reduction. Comptes Rendus Geosci 2006;338(6–7):456–67.
[86] Rolle M, Clement TP, Sethi R, Di Molfetta A. A kinetic approach for simulating redox-controlled fringe and core biodegradation processes in groundwater: model development and application to a landfill site in Piedmont, Italy. Hydrol Process 2008;22:4905–21.
[87] Rosner BM, McCarty PL, Spormann AM. In vitro studies on reductive vinyl chloride dehalogenation by an aerobic mixed culture. Appl Environ Microbiol 1997;63(11):4139–44.
[88] Roychowdhury S, Cox D, Levandowsky M. Production of hydrogen by microbial fermentation. Int J Hydrogen Energy 1988;13(7):407–10.
[89] Schäfer D, Schäfer W, Kinzelbach W. Simulation of reactive processes related to biodegradation in aquifers: 1. Structure of the three-dimensional reactive transport model. J Contam Hydrol 1998;31(1–2):167–86.
[90] Seagren EA, Rittmann BE, Valocchi AJ. Quantitative evaluation of the enhancement of NAPL-pool dissolution by flushing and biodegradation. Environ Sci Technol 1994;28(5):833–9.
[91] Semprini L, McCarty PL. Comparison between model simulations and field results for in-situ biorestoration of chlorinated aliphatics: Part2. Cometabolic Transformations. Ground Water 1992;30(1):37–44.
[92] Schöllhorn A, Savary C, Stucki G, Hanselmann W. Comparison of different substrates for the fast reductive dechlorination of trichloroethene under groundwater conditions. Water Res 1997;31(6):1275–82.
[93] Sharma PK, McCarty PL. Isolation and characterization of a facultatively aerobic bacterium that reductively dehalogenates tetrachloroethene to cis-1,2-dichloroethene. Appl Environ Microbiol 1996;62(3):761–5.

[94] Sleep BE, Sykes JF. Compositional simulation of groundwater contamination by organic compounds. 1, Model development and verification. Water Resour Res 1993;29(6):1697–708.
[95] Sleep BE, Sykes JF. Compositional simulation of groundwater contamination by organic compounds. 2. Model applications. Water Resour Res 1993;29(6):1709–18.
[96] Sleep BE, Brown AJ, Lollar BS. Long-term tetrachloroethene degradation sustained by endogenous cell decay. J Environ Eng Sci 2005;4(1):11–7.
[97] Stanners D, Bourdeau P, editors. Europe's environment—the Dobris assessment. Copenhagen: European Environment Agency; 1995.
[98] Stucki G, Hanselmann KW, Hurzeler RA. Biological sulphuric acid transformation: reactor design and process optimization. Biotechnol Bioeng 1993;41(3):303–15.
[99] Sung Y, Ritalahti KM, Sanford RA, Urbance JW. Characterization of two tetrachloroethene-reducing, acetate-oxidizing anaerobic bacteria and their description as *Desulfuromonas michiganensis* sp. nov. Appl Environ Microbiol 2003;69(5):2964–74.
[100] Tandoi V, DiStefano TD, Bowser PA, Gossett JM, Zinder SH. Reductive dehalogenation of chlorinated ethenes and halogenated ethanes by a high-rate anaerobic enrichment culture. Environ Sci Technol 1994;28(5):973–9.
[101] Taylor SW, Jaffe PR. Biofilm growth and the related changes in the physical properties of a porous medium: 1. Experimental investigation. Water Resour Res 1990;26(9):2153–9.
[102] Taylor SW, Milly PCD, Jaffe PR. Biofilm growth and the related changes in the physical properties of a porous medium: 2. Permeability. Water Resour Res 1990;26(9):2161–9.
[103] Thauer RK, Möller-Zinkhan D, Spormann AM. Biochemistry of acetate catabolism in anaerobic chemotrophic bacteria. Ann Rev Microbiol 1989;43:43–67.
[104] Vandevivere P, Baveye P. Saturated hydraulic conductivity reduction caused by aerobic bacteria in sand columns. Soil Sci Soc Am J 1992;56(1):1–13.
[105] Westrick JJ, Mellow JW, Thomas RF. The groundwater supply survey. J Am Water Works Assoc 1984;76(5):52–9.
[106] Widdel F. Microbiology and ecology of sulfate- and sulfur-reducing bacteria. In: Zehnder AJB, editor. Biology of anaerobic microorganisms. New York: Wiley; 1998. p. 469–586.
[107] Widdowson MA. Modelling natural attenuation of chlorinated ethenes under spatially varying redox conditions. Biodegradation 2004;15(6):435–51.
[108] Yang Y, McCarty PL. Competition of hydrogen within a chlorinated solvent dehalogenating anaerobic mixed culture. Environ Sci Technol 1998;32(22):3591–7.
[109] Yang Y, McCarty PL. Biologically enhanced dissolution of tetrachloroethene DNAPL. Environ Sci Technol 2000;34(14):2979–84.
[110] Yang Y, McCarty PL. Biomass, oleate, and other possible substrates for chloroethene reductive dehalogenation. Biorem J 2000;4(2):125–33.
[111] Yang Y, McCarty PL. Comparison between donor substrates for biologically enhanced tetrachloroethene DNAPL dissolution. Environ Sci Technol 2002;36(15):3400–4.
[112] Younesi H, Najafpour G, Mohamed AR. Ethanol and acetate production from synthesis gas via fermentation processes using anaerobic bacterium, *Clostridium ljungdahlii*. Biochem Eng J 2005;27(2):110–9.
[113] Yeh HC, Kastenberg WE. Health risk assessment of biodegradable volatile organic chemicals. A case study of PCE, TCE, DCE and VC. J Hazard Mater 1991;27(2):111–26.
[114] Yu S. Kinetics and modeling investigations of the anaerobic reductive dechlorination of chlorinated ethylenes using single and binary mixed cultures and silicon-based organic compounds as slow release substrates. Ph.D. Thesis, Oregon State University, Corvallis, 2003.
[115] Yu S, Semprini L. Kinetics and modeling of reductive dechlorination at high PCE and TCE concentrations. Biotechnol Bioeng 2004;88(4):451–64.
[116] Yu S, Dolan ME, Semprini L. Kinetics and inhibition of reductive dechlorination of chlorinated ethylenes by two different mixed cultures. Environ Sci Technol 2005;39(1):195–205.
[117] Zhuang P, Pavlostathis SG. Effect of temperature, pH and electron donor on the microbial reductive dechlorination of chloroalkes. Chemosphere 1995;31(6):3537–48.